HHS Public Access

Author manuscript

J Comp Neurol. Author manuscript; available in PMC 2021 September 01.

Published in final edited form as:

J Comp Neurol. 2020 September 01; 528(13): 2174–2194. doi:10.1002/cne.24883.

Characterization of Drosophila octopamine receptor neuronal expression using MiMIC-converted Gal4 lines

Hannah M. McKinney[1], **Lewis M. Sherer**[2], **Jessica L. Williams**[1,3], **Sarah J. Certel**[2,4], **R. Steven Stowers**[1]

[1]Department of Cell Biology and Neuroscience, Montana State University, Bozeman, Montana

[2]Cellular, Molecular and Microbial Biology Graduate Program, The University of Montana, Missoula, Montana

[3]Department of Plant Sciences, Montana State University, Bozeman, Montana

[4]Division of Biological Sciences, Center for Structural and Functional Neuroscience, The University of Montana, Missoula, Montana

Abstract

Octopamine, the invertebrate analog of norepinephrine, is known to modulate a large variety of behaviors in *Drosophila* including feeding initiation, locomotion, aggression, and courtship, among many others. Significantly less is known about the identity of the neurons that receive octopamine input and how they mediate octopamine-regulated behaviors. Here, we characterize adult neuronal expression of MiMIC-converted Trojan-Gal4 lines for each of the five *Drosophila* octopamine receptors. Broad neuronal expression was observed for all five octopamine receptors, yet distinct differences among them were also apparent. Use of immunostaining for the octopamine neurotransmitter synthesis enzyme Tdc2, along with a novel genome-edited conditional *Tdc2-LexA* driver, revealed all five octopamine receptors express in Tdc2/octopamine neurons to varying degrees. This suggests autoreception may be an important circuit mechanism by which octopamine modulates behavior.

Keywords

autoreception; Drosophila; octopamine; octopamine receptor; RRID:AB_221568; RRID:AB_2340686; RRID:AB_2340850; RRID:AB_2536611; RRID:AB_2633280; RRID:AB_2814891; RRID:BDSC_27392; RRID:BDSC_42119; RRID:BDSC_43050; RRID:BDSC_57940; RRID:BDSC_59133; RRID:BDSC_60312; RRID:BDSC_60313; RRID:BDSC_67636; RRID:BDSC_68264

Correspondence R. Steven Stowers, Department of Cell Biology and Neuroscience, Montana State University, Bozeman, MT., sstowers@montana.edu.

DATA AVAILABILITY STATEMENT

Complete sequences of donor plasmids are shown in Supplemental Information. Fly strains original to this publication will be deposited at the Bloomington Drosophila stock center or will be made available upon request. Donor plasmids will be deposited at Addgene or will be made available upon request.

SUPPORTING INFORMATION

Additional supporting information may be found online in the Supporting Information section at the end of this article.

1 | INTRODUCTION

The vertebrate adrenergic system is integral to countless behavioral and physiological processes, including stress response (Snyder & Silberman, 2019), metabolic maintenance (Ciccarelli, Sorriento, Coscioni, Iaccarino, & Santulli, 2016), and neuropsychiatric diseases (Langer, 2015; Sallee, Connor, & Newcorn, 2013). Adrenergic signaling occurs via the release of adrenaline (epinephrine) and noradrenaline (norepinephrine). Both adrenaline and noradrenaline exert their various effects by binding to G-protein coupled receptors (GPCRs). These receptors are classified as either α-adrenergic or β-adrenergic and trigger numerous downstream signaling events, including the activation of protein kinases and increased gene transcription, through the second messengers cyclic AMP (cAMP) and calcium (Ca^{2+}) (Ciccarelli et al., 2016; Cole & Sood, 2012; Santulli & Iaccarino, 2013; Vaniotis et al., 2011). In addition to the complexity of downstream signaling, the location of adrenergic receptors is multifaceted with receptors located presynaptically as well as postsynaptically (Langer & Angel, 1991). While many studies in recent decades have examined the role of postsynaptic adrenergic receptors, the impact of presynaptic receptors, or *autoreceptors*, on circuits that regulate behavior and as targets for drug discovery remains poorly examined.

Drosophila melanogaster offers several advantages to investigating adrenergic receptor localization and function including a sophisticated genetic toolbox, a simpler nervous system, and a reduced number of neurotransmitter receptors as compared to vertebrates. In *Drosophila*, octopamine (Oct), the structural analogue of norepinephrine, is synthesized from the amino acid tyrosine via the action of tyrosine decarboxylase (Tdc) and tyramine-ß-hydroxylase (Roeder, 1999). Oct exerts its effects by binding to Oct receptors (OctRs), including five adrenergic-like receptors in *Drosophila*: two α-adrenergic-like GPCRs (OAMB and Octα2R) and three β-adrenergic-like GPCRs (Octβ1R, Octβ2R, and Octβ3R) (Balfanz, Strunker, Frings, & Baumann, 2005; El-Kholy et al., 2015; Evans & Maqueira, 2005; Han, Millar, & Davis, 1998; Maqueira, Chatwin, & Evans, 2005; Qi et al., 2017).

Presynaptic autoreceptors provide a retrograde transfer of information mediated by the released transmitter of the presynaptic neuron and can perform autoregulatory functions in neurotransmission. For example, at the *Drosophila* neuromuscular junction (NMJ), activation of Octβ2R autoreceptors is required for the growth of Oct arbors during development and in response to starvation, while the inhibition of this synaptic growth depends on the autoreceptor function of Octβ1R (Koon et al., 2011; Koon & Budnik, 2012). Autoreception may also provide a critical component in regulating the activity of neurons that release more than one neurotransmitter, neuropeptide or neuromodulator, such as neurons expressing dopamine and the vesicular glutamate transporter (Aguilar et al., 2017). Most recently, it has been shown that the majority of octopaminergic neurons also express glutamate (Sherer et al., in press). As dual neurotransmitter usage is now recognized to occur throughout the nervous system of invertebrates and vertebrates (Hoopfer, 2016; Nassel, 2018; Seal & Edwards, 2006; Vaaga, Borisovska, & Westbrook, 2014), elucidating the role of the corresponding neurotransmitter receptors, including as autoreceptors, is important for understanding of the functionality of dual transmitter neurons.

As a precursor to addressing the functional impact of OctR presynaptic and postsynaptic signaling on Oct transmission, we first sought to determine the neuronal expression patterns of Drosophila OctRs. Our approach was to generate Trojan-Gal4 lines for *OAMB, Octβ1R, Octβ2R,* and *Octβ3R* through MiMIC conversion (Diao et al., 2015). MiMIC converted Gal4 drivers faithfully recapitulate the cellular expression of their corresponding genes (Diao et al., 2015) as they are located at the endogenous chromosomal locus of their respective genes and thus the complete regulatory region of each gene directs their expression. Here, we characterized the adult central nervous system expression patterns of each new *OctR-Gal4* line along with the *Octα2R* Trojan-Gal4 from the Gene Disruption Project (Li-Kroeger et al., 2018), and examined *OctR* autoreception expression in Tdc2 neurons. To further refine our autoreceptor analysis, we generated new intersectional genetic tools for *Tdc2* and the *Drosophila* non-NMDA ionotropic glutamate receptor *DmGluR1A* (Ultsch et al., 1992) to provide a genetic means of identifying co-expression with OctRs. Each OctR exhibited unique autoreceptor expression patterns using both antibody staining and genetic approaches. We also identified a number of neurons co-expressing *OctRs* and *GluRIA*, thus indicating the potential convergence of dual Oct-glutamate signals to the same downstream target neurons. Our new tools provide novel intersectional methods to use in further identifying and understanding the complexities of adrenergic receptor signaling and localization.

2 | MATERIALS AND METHODS

Plasmid construction

The *pCFD4-Tdc2* and *pCFD4-GluRIA* double guide RNA plasmids were generated as previously described (Port, Chen, Lee, & Bullock, 2014). Targeting sequences included in *pCFD4-Tdc2* guide RNAs are CATAATAAAGCTCACCGT and AAATCTTTTATAGGACGA. Targeting sequences included in *pCFD4-GluRIA* guide RNAs are GGCGAGCC CAGGCGAATT and GCCATGGCTCGTTGGGGA. Donor plasmids were constructed with NEBuilder HiFi (New England Biolabs) in the vector *pHSG298* (Takara Biosciences). The complete sequences of all donor plasmids are shown in Supplemental Information.

The *20XUAS-DSCP-KD, 20XUAS-B3, 10XQUAS-DSCP-His2B-mCherry,* and *10XUAS-DSCP-His2A-GFP* expression clones were assembled using Gateway MultiSite cloning as previously described (Petersen & Stowers, 2011). The *L1-10XQUAS-DSCP-L5* entry clone was generated using the *L1-10XQUAS-L4* entry clone (Petersen & Stowers, 2011) as template such that the *hsp70* minimal promoter was replaced with the Drosophila synthetic core promoter (DSCP) (Pfeiffer et al., 2008). The table below includes fly lines created for publication in this article.

Genome-edited Fly Strains **B3RT-Tdc2-LexA** **KDRT-GluRIA-QF2**	
Transgenic Fly Strains	Landing Site
LexAop2-6XmCherry	*JMK66B*
UAS-His2A-GFP	*VK18* (53B), *VK5* (75A)
LexAop2-His2B-mCherry	*JMK66B*
UAS-KD	*VK18* (53B)
UAS-B3	*VK31* (62E)
QUAS-His2B-mCherry	*VK2* (28E)

Genome editing

The *pCFD4-Tdc2* guide RNA plasmid was co-injected with the *B3RT-TDC2-LexA* donor plasmid into embryos of strain *nos-Cas9 TH_attP2* (Ren et al., 2013) by Bestgene, Inc. The surviving adults that were injected as embryos were crossed to *yw; UAS-B3; n-syb-GAL4, LexAop2-6XmCherry* and genome-edited *B3RT-TDC2-LexA* chromosomes were identified by fluorescence. The observation that the *B3RT-Tdc2* female is homozygous sterile suggests the function of the *Tdc2* gene is likely disrupted prior to excision as this is the phenotype of the octopamine null mutant (Monastirioti, 2003). Nevertheless, *B3RT-Tdc2* remains a reliable and valid tool for identifying Tdc2 neurons. The *pCFD4-GluRIA* guide RNA plasmid was co-injected with the *KDRT-GluRIA-QF2* donor plasmid into embryos of strain *nos-Cas9 TH_attP40* (Ren et al., 2013) by Bestgene, Inc. The surviving adults that were injected as embryos were crossed to *yw; N-syb-GAL4; UAS-B3, LexAop2-6XmCherry* and genome-edited *KDRT-GluRIA-QF2* chromosomes were identified by fluorescence.

Germline excisions and inversions

Germline excisions were generated by crossing *B3RT-Tdc2-LexA* to *yw; nos-GAL4; UAS-DSCP-B3* and *KDRT-GluRIA-QF2* to *yw; nos-GAL4; 20XUAS-DSCP-KD.* Progeny males of the appropriate genotype were crossed to a second chromosome balancer stock to generate individual flies with potential germline excisions. Germline excisions were identified by taking individual males from the first balancer cross and crossing them to a *13XLexAop2-6XmCherry-HA* or *10XQUAS-6XmCherry-HA* fluorescent reporter and screening directly for fluorescence. Balanced fly stocks containing the desired germline excised or inverted chromosomes were established from progeny of positive single male crosses.

Fly strains/MiMIC lines

A table of original fly lines used in this paper can be found in the Supplemental Information. Flies were raised on standard cornmeal, yeast and agar food at 25°C and occasionally kept at 18°C after sorting and prior to dissection. MiMIC lines OAMB (BDSC #57940); *Octβ1R* (BDSC #42119); *Octβ2R* (BDSC #59133); *Octβ3R* BDSC #43050) were converted to Trojan-Gal4 lines following recombinase-mediated cassette exchange as described in Diao et al. (2015). *Octα2R-Gal4* (BDSC #67636), *vGlut-Gal4* (BDSC #60312) *Tdc2*-Gal4-AD

(BDSC #68264) and *vGlut*-Gal4-DBD (BDSC # 60313), and *UAS-CD8-mCherry* (F. Schnorrer, BDSC# 27392) were obtained from the Bloomington Drosophila Stock Center.

2.1 | Immunostaining—Immunostaining was performed as previously described (Certel & Thor, 2004). Primary antibodies and dilution factors: The SYN (3C11) mAb 1:50 developed by Buchner (Klagges et al., 1996), anti-bruchpilot (nc82) mAb 1:30 developed by Buchner were obtained from the Developmental Studies Hybridoma Bank, created by the NICHD of the NIH and maintained at The University of Iowa, Department of Biology, Iowa City, IA 52242; rabbit Abfinity anti-GFP (Thermo-Fisher) 1:400, mouse anti-GFP 3E6 (Thermo-Fisher) 1:200, rat anti-mCherry 16D7 (Thermo-Fisher) 1:400, rabbit anti-mCherry (Abcam ab213511) 1:500, mouse anti-mCherry 1:400 (Biorbyt orb256058); rat anti-GFP 8H12 (Kerafast) 1:200; rabbit anti-Tdc2 (pab0822-P, Covalab) 1:400 and 1:200). Secondary antibodies and dilution factors: donkey anti-mouse Alexa 488 (Jackson Immunoresearch 715-546-151) 1:400; goat anti-rabbit Alexa 488 (Thermo-Fisher A32731) 1:400; donkey anti-rat Alexa 488 (Jackson 712-546-153) 1:400; goat anti-rabbit JF549 (Novus NBP1-72732JF549) 1:200; donkey anti-mouse JF549 (Novus NBP1-75119JF549) 1:200; goat anti-rat JF549 (Novus NBP1-75398JF549) 1:200; goat anti-rabbit JF646 (NBP1-72732JF646) 1:200; donkey anti-mouse JF646 (Novus NBP1-75119JF646) 1:200, and goat anti-rat JF646 (Novus NBP1-75398JF646) 1:200.

3 | RESULTS

Earlier generation *OctR-Gal4* drivers utilized only one to three kilobases of *OctR* promoter regions (El-Kholy et al., 2015), even though each of the *OctR* genes span tens of kilobases in the *Drosophila* genome. As such, the respective regulatory regions are likely more extensive, making it probable that existing *OctR-Gal4* lines provide incomplete *OctR* expression patterns. Additionally, as with all transgenes, the existing *OctR-Gal4* lines are potentially subject to position effects associated with transgenic insertion sites. To more accurately recapitulate the complete neuronal expression pattern of *Drosophila* OctRs as a precursor to functional studies, we generated Trojan-Gal4 lines for *OAMB, Octβ1R, Octβ2R,* and *Octβ3R* using the previously described cross scheme (Diao et al., 2015) and examined their expression patterns using both nuclear (*UAS-His2A-GFP*; Figure 1a1–a5) and plasma membrane (*UAS-CD-mCherry*; Figure 1c1–c5) markers. These drivers likely are complete and accurate reporters of the transcriptional expression of their respective *OctR* genes since the Trojan-GAL4 lines are located at the endogenous genomic location of each OctR gene within coding introns common to all isoforms (Figure 1b1–b5). As such, they represent the "gold standard" for reporting on the complete expression pattern of a gene (Diao et al., 2015). It is worth noting, however, that translational regulation of OctR protein expression cannot be ruled out and thus could differ from the patterns reported here using fluorescent reporters. Additional advantages of these lines include the absence of position effects and the detection of *OctR* gene expression with higher sensitivity and higher fidelity.

3.1 | Tdc2 and *OctR* co-expression

To assess the possibility of OctR autoreception in the central brain, we mapped *OctR* expression in octopaminergic neurons using two approaches. First, we expressed a UAS-

driven nuclear GFP reporter via the individual *OctR-Gal4* lines and analyzed Oct/tyramine co-expression with an antibody against Tdc2. As Oct is synthesized from the amino acid tyrosine via the action of Tdc2 and Tβh in invertebrates (Cole et al., 2005), the Tdc2 antibody (Meiselman, Kingan, & Adams, 2018; Pauls, Blechschmidt, Frantzmann, El Jundi, & Selcho, 2018; Pech, Pooryasin, Birman, & Fiala, 2013) recognizes neurons that express Oct and/or tyramine (hereafter "Tdc2+ neurons" for simplicity).

Second, we utilized a novel intersectional genetic method to label Tdc2-expressing neurons and determine co-expression with each *OctR-Gal4* driven reporter. For each *OctR-Gal4*, at least 25 adult brains were examined per genotype and the representative nuclear expression pattern in anterior and posterior sections is shown. Results from both methods revealed significant coexpression of Tdc2 and *OctR*'s, suggesting putative locations for autoreception.

3.2 | Oct α-adrenergic receptors: OAMB and Octα2R

Oct neurons in the adult *Drosophila* brain are located in discernible clusters (Busch et al., 2009) throughout anterior and posterior sections (Figure 2a1–a3). Our newly generated *OAMB-Gal4* line drives nuclear GFP expression as expected in the mushroom body Kenyon cells (El-Kholy et al., 2015; Han et al., 1998) as well as broadly throughout the rest of the brain (see Figure 2b–g3) and VNC (Figure 2h1–i3). In anterior sections of the brain, Tdc2 and His2A-GFP nuclear expression driven by *OAMB-Gal4* (henceforth *OAMB > His2A-GFP*) are co-expressed within the ASM cluster of Tdc2+ neurons (Figure 2c1–c3, closed arrows), which is located superior to the antennal lobes (AL) (Figure 2a2). Within this cluster, *OAMB > His2A-GFP* was not found in two pairs of Tdc2+ neurons (Figure 2c1-c3, open arrows). Tdc2 and *OAMB > His2A-GFP* were co-expressed in the VL neurons, located between the AL and the ventrolateral protocerebrum (Figure 2a2, see Figure 7). Co-expression was not detected in the anterior or posterior subesophageal ganglion (SEZ; Figure 2d1–d3, f1–f3, open arrows) or in the PB1 cluster of Tdc2+ neurons in the posterior superior medial protocerebrum (PSMP; Figure 2g1–g3, open arrows).

Similar to *OAMB*, we found *Octα2R-Gal4* driven His2A-GFP (*Octα2R > His2A-GFP*) expression widespread throughout the brain (Figure 3a,b) and VNC (Figure 3e1–f3). *Octα2R > His2A-GFP/Tdc2* co-expression was seen within the majority of ASM Tdc2+ neurons, and in the SEZ and AL2 neurons (Figure 3c1–c3, closed white arrows). Examination of single confocal sections of the VNC revealed a number of neurons showing co-expression with Tdc2 (Figure 3f1–f3, closed white arrows) and a number of Tdc2+ neurons lacking His2A-GFP expression (Figure 3f1–f3, closed white arrow). In contrast to the absence of OAMB/Tdc2 co-expression in the SEZ, *Octα2R > His2A-GFP* is co-expressed in the majority of Tdc2+ neurons in the SEZ (Figure 3c1–d3, closed arrows) with the exception of one pair in the posterior SEZ (Figure 3d1–d3, open arrows). Co-expression was also detected in the PSM and VL clusters (see Figure 7). The identification of distinct clusters of alpha-adrenergic autoreceptor expression indicates potential key areas of functional differences.

3.3 | Oct β-adrenergic receptors: Octβ1R, Octβ2R, and Octβ3R

His2A-GFP expression driven by *Octβ1R-Gal4* (*Octβ1R > His2A-GFP*) was widespread throughout the central brain, including the Kenyon cells (Figure 4a,b), and the VNC (Figure 4f1–g3). In contrast to *OAMB*, Tdc2 and *Octβ1R > His2A-GFP* were co-expressed in the AL1, PB1 and VM clusters of Tdc2+ neurons (Figure 4c1–d3). Within the AL clusters, there were a number of co-expressing neurons (Figure 4c1–c3, closed arrows) and at least one neuron with no co-expression (Figure 4c–c2, open arrow). In the posterior and anterior sections of the SEZ, *Octβ1R > His2A-GFP* exhibited co-expression with Tdc2 (Figure 4e–e2). At least one neuron in the VNC of *Octβ1R > His2A-GFP* co-expressed with Tdc2 (Figure 4f1–f3, closed white arrow) while the majority of neurons in the VNC did not co-express with Tdc2 (Figure 4g1–g3, open white arrow).

Octβ2R-Gal4 driven His2A-GFP expression (*Octβ2R > His2A-GFP*; Figure 5a–c) was detected with Tdc2 in all Tdc2+ neuron clusters in the adult brain (Figure 5d–h2) and only one neuron in the VNC (Figure 5i1–j3, closed white arrow). Several pairs of Tdc2+ neurons in the ASM cluster co-expressed Tdc2 and *Octβ2R > His2A-GFP*, with at least one pair negative for co-expression (Figure 5d1–d3). A significant amount of co-expression was observed in the AL2 cluster of the AL (Figure 5e1–e3, closed white arrows), however *Octβ2R > His2A-GFP* was not detected in AL1 neurons (Figure 5e1–e3, open arrows). At least two VM neurons in the SEZ co-expressed *Octβ2R > His2A-GFP* and Tdc2 (Figure 5g1–g3), with co-expression also seen in PB1 cluster of the PSMP region (Figure 5h1–h3, closed white arrow).

Figure 6 illustrates the widespread neuronal expression of His2A-GFP driven by the *Octβ3R-Gal4* (*Octβ3R > His2A-GFP*; Figure 6a,b). *Octβ3R > His2A-GFP* co-expression with Tdc2 was detected in several Tdc2+ neuronal clusters, including both the anterior and PSMP of adult brains (Figure 6c1–d3, closed white arrows) and in at least one neuron in the VNC (Figure 6f1–f3, closed white arrow). Lack of co-expression was also seen in the PSMP (Figure 6d1–d3, open white arrows) and in the VNC (Figure 6f1–f3, open white arrows).

3.4 | Sex differences in *OctR-Gal4* expression

Levels of Octα2R mRNA in particular have been reported to be higher in males than females (Qi et al., 2017). This difference could reflect a greater number of Octα2R-expressing neurons in males or sex-specific differences in gene expression. We thus decided to examine differences between males and females in every *OctR-Gal4* line and also observe any differences in their co-expression with the Tdc2 antibody (Figure 7). While neuron count was not quantified, no gross differences in *Gal4 > His2A-GFP* expression patterns were seen between males and females (Figure 7a1–j2). However, we did determine *Octα2R > His2A-GFP* expression in females co-localized with Tdc2 in the posterior SEZ (Figure 7d2, closed white arrow) while in males *Octα2R > His2A-GFP* expression was not detectable in this pair of Tdc2+ VM neurons (Figure 7c2, open white arrow). These results indicate potential sex-specific differences in α-adrenergic autoreceptor expression and suggest an area for further study. In summary, we have generated new *OctR-Gal4* lines and determined each OctR has the potential to serve an autoregulatory function due to co-expression within distinct Tdc2+ clusters.

3.5 | *B3RT-Tdc2-LexA* intersectional genetics confirms potential autoreceptor locations

As shown above with the MiMIC *OctR-Gal4*s, distinct presynaptic receptor expression was observed for each OctR. To independently assess the overlap of *OctR* expression with Tdc2+ neurons, a variant of *Tdc2, B3RT-Tdc2-LexA* (hereafter *B3RT-Tdc2*), was developed via CRISPR/Cas9 genome editing (see Section 2). *B3RT-Tdc2* incorporates one B3 recombinase target site, *B3RT*, (Nern, Pfeiffer, Svoboda, & Rubin, 2011) into the 5′ untranslated region (UTR) of the *Tdc2* genomic locus, and a second *B3RT* adjacent to the coding sequence of the LexA transcription factor in an intron between the first two coding exons (Figure 8a). Prior to excision of the DNA between the *B3RT*s, LexA is not expressed, but after excision, a *Tdc2-LexA* driver results. Thus, intersectional expression between any Gal4 driver and *Tdc2* neurons can be revealed using *B3RT-Tdc2* in combination with a *UAS-B3* recombinase transgene and a *LexAop* reporter. Since *B3RT* excisions are effectively permanent, any neurons experiencing excisions during development will retain those excisions in the adult, even if Gal4 expression is not maintained. *LexAop* reporter expression that does not also show *UAS* expression may thus be observed with some Gal4 drivers as a result of excisions that occurred during development. No *LexAop2* reporter expression was detected in the absence of a Gal4 driver (Figure 8b), thus indicating neither the *UAS-B3* recombinase nor *LexAop2–6XmCherry* reporter exhibits leaky expression.

To assess whether the *B3RT-Tdc2* recapitulates endogenous expression of *Tdc2*, a germline excision of B3RT-Tdc2 was generated and the resulting *LexAop2–6XmCherry* reporter expression was compared to endogenous Tdc2 protein expression. Neuronal expression of the 6XmCherry reporter recapitulates Tdc2 expression (Figure 8c1–c3), as expected for genome editing at the endogenous chromosomal locus of *Tdc2* with its complete regulatory region. A similar *Tdc2* neuronal expression pattern was also observed upon panneuronal excision using the *n-syb-Gal4* driver and the *LexAop2-His2Bm-Cherry* reporter (Figure 8d1–d3), thus indicating B3 recombinase-mediated excision occurs with a high level of efficiency.

After verifying that both the germline excision and pan-neuronal excision of *B3RT-Tdc2* closely recapitulated endogenous Tdc2 expression, we utilized this method to further assess overlapping expression of Tdc2 and OctRs. To visualize *Tdc2* and *OctR* co-expression, we utilized the same *UAS-His2A-GFP* nuclear reporter for all *OctR-Gal4*s and the *LexAop2-His2BCherry* nuclear reporter to reveal conditional *B3RT-Tdc2* expression (Figure 6e1–f3, Figure 7). *B3RT-Tdc2 > His2B-mCherry* labeled a similar pattern of neurons in the intersection of the *OAMB-Gal4* and *B3RT-Tdc2* as was seen with the Tdc2 antibody (Figure 8e1–e3, compare to Figure 2b–g3), including the VL neurons and those within the ASM cluster. Likewise, driving B3 recombinase with *Octα2R-Gal4* resulted in co-expression of His2B-mCherry and His2A-GFP in both pairs of VL neurons, as well as neurons within the AL, the ASMP and PSMP clusters, and the SEZ (Figure 8f1–f3).

B3RT-Tdc2 also corroborated the overlapping expression of Tdc2 with each *OctβR-Gal4* (Figure 9a1–c3), demonstrating co-expression in the PSMP, ASMP, AL (with *Octβ3R* exhibiting the least on average, of the *OctβR-Gal4*s; see Figure 9b), and VM clusters of Tdc2+ neurons, closely recapitulating results seen with the Tdc2 antibody and *OctR* co-expression in Figures 4–7. Using the nuclear reporters with the *B3RT-Tdc2* method also

allowed us to manually count co-expressing *OctR-Tdc2* neurons with greater ease than with antibody staining (Figure 10). In the ASMP, *Octα2R-Gal4* had the lowest average of co-expressing neurons (Figure 10a), though *Octα2R-Gal4* showed the highest average of co-expression in the antennal lobe, followed by *Octβ1R-Gal4* (Figure 10b). In the SEZ, *OAMB-Gal4* had the lowest average of co-expressing neurons with *B3RT-Tdc2,* with *Octα2R-Gal4* again having the highest average, followed by *Octβ2R-Gal4*. All *OctR-Gal4*s co-expressed neurons in low numbers in the PSMP, with *OAMB-Gal4* co-expressing the least on average (Figure 10d). However, within the lateral clusters of the Tdc2+ neurons, *Octβ2R-Gal4* co-expressed the least (Figure 10e). In summary, *B3RT-Tdc2* independently confirms the co-expression observed using the Tdc2 immunostaining approach and also demonstrates its utility for identifying *Tdc2* neurons whose expression overlaps that of a Gal4 driver of interest.

3.6 | Intersectional genetics reveals co-expression of two types of receptors

We recently demonstrated that Oct neurons in the adult brain co-express the *Drosophila* vesicular glutamate transporter (dVGlut) (Sherer et al., in press) (Figure 11a). In addition, single-cell transcriptomics data demonstrate a high percentage of mid-brain Oct-expressing neurons also express markers for dVGlut (Croset, Treiber, & Waddell, 2018). The functional capabilities of such dual neurotransmission neurons are complex. For example, the postsynaptic response to Oct and glutamate may be determined by neurons expressing receptors for one or both neurotransmitters. In an initial attempt to determine whether glutamate and octopamine receptors are expressed in the same neurons, co-expression between OctRs and the *Drosophila* non-NMDA ionotropic glutamate receptor, GluRIA (Ultsch et al., 1992) was investigated.

As the intersectional genetic approach provides a powerful means to assess co-expression, we used CRISPR/Cas9 genome editing to generate a conditional *GluRIA* allele, *KDRT-GluR1A-QF2* (hereafter *KDRT-GluR1A*) at the endogenous GluR1A chromosomal locus. *KDRT-GluR1A* is analogous to *B3RT-Tdc2* described above except it uses KD recombinase target sites (*KDRTs*) (Nern et al., 2011) and the QF2 transcription factor (Riabinina & Potter, 2016). *KDRT-GluR1A* contains one *KDRT* in the 5′ UTR and a second *KDRT* with adjacent QF2 coding sequences in the intron between the first two coding exons of *GluR1A*. Prior to excision, the QF2 driver is not expressed (Figure 11b). However, after pan-neuronal KD recombinase-mediated excision using the *n-syb-Gal4*, a *GluR1A-QF2* driver is created that expresses broadly in the optic lobes and sparsely in the central brain (Figure 11c1,c2). This pattern is highly similar to the pattern observed in a *KDRT-GluR1A* germline excision (Figure 11d), indicating KD recombinase-mediated excisions occur with high efficiency. *KDRT-GluRIA* can thus be used to reveal intersectional expression of any Gal4 driver with GluRIA neurons. Additionally, *KDRT-GluR1A* can be used to remove GluR1A receptor function in individual neurons.

Images demonstrating the intersection of the expression of *OctR > His2A-GFP* and *KDRT-GluRIA > His2B-mCherry* in anterior sections of the brains are shown in Figures 11 and 12. The *OAMB* receptor and *KDRT-GluRIA* are co-expressed in neurons surrounding the SEZ, a region that contains many Oct neurons and receives chemosensory information, as well as

two neurons in the superior medial protocerebrum (SMP) and four neurons within the periesophageal neuropils (PENP) (Figure 11e1–e3, closed white arrow). *Octα2R > His2A-GFP* neurons that co-express *KDRT-GluRIA > His2B-mCherry* are also found in the central brain within the medial area of the SEZ as well as SMP and PENP neurons (Figure 11f1–f3, closed white arrow).

The co-expression of *OctβR*'s and *KDRT-GluRIA* ranges from a small number of neurons to widespread co-expression (e.g., *Octβ3R-Gal4*), suggesting the possibility of key differences in neurons that have the potential to respond to both octopamine and glutamate signaling (Figure 9). *KDRT-GluRIA* and *Octβ1R* or *KDRT-GluRIA* and *Octβ2R* were co-expressed in neurons located in the SEZ and ventro-medial to the AL (Figure 12a1–b3, closed white arrows). *Octβ3R* and *KDRT-GluRIA* are broadly co-expressed in the central brain and optic lobes (Figure 12c1–d3, closed white arrows). Co-expression was observed in the SMP, the superior lateral protocerebrum, the PENP, and posterior lateral protocerebrum (Figure 12d1–d3). The *Octβ3R-Gal4* was the only OctR that showed substantial co-expression with *KDRT-GluRIA* in the posterior sections of the brain (Figure 12d–d2). These results indicate widespread differences in the co-expression of *OctRs* and *GluRIA*.

As these results indicate substantial evidence for Oct autoreceptor usage, we decided to also investigate GluRIA potential autoreception within Oct-Glut dual transmitting neurons seen in Figure 11a. Although less common, glutamate receptors have also been known to function as autoreceptors (Pittaluga, 2016). A *Tdc2−/vGlut-* split *Gal4* line, which labels all neurons expressing both *Tdc2* and *vGlut* (Figure 9e3), crossed to our *KDRT-GluRIA* labeled an average of 11.5 dual transmitting neurons in the SEZ that also express *GluRIA* (Figure 12e1–e3, closed white arrows, $n = 6$). This result indicates these dual transmission SEZ neurons may use presynaptic glutamate receptors as autoreceptors. The schematic in Figure 10 offers plausible scenarios for both pre- and postsynaptic signaling from dual transmission neurons. On the presynaptic side (Figure 13a–c), synaptic vesicles of dual transmitting neurons may release neurotransmitters from the same (Figure 13a) or separate (Figure 13b,c) synaptic vesicles and this release may also be spatially segregated (Hnasko & Edwards, 2012). Our results demonstrate Oct presynaptic receptor localization, which is likely utilized for autoreceptor presynaptic signal regulation as seen in Figure 13a,c. Our data also suggest the possibility of a presynaptic glutamate autoreceptor (Figure 13a). Downstream from dual Oct-Glut neurons, postsynaptic neurons may express receptors for Oct or Glut (Figure 13b,c) or as our results also indicate, downstream neurons can express both an OctR and a GluR, (Figure 13a). Using the new intersectional genetic tools described here, further studies will be able to address the function of presynaptic and postsynaptic receptor localization on octopamine signaling.

4 | DISCUSSION

In this study, we used MiMIC Trojan-Gal4 lines for each of the five OctRs to characterize *OctR* expression in Drosophila. Broad expression of each *OctR* receptor was observed throughout the adult brain and VNC, including in Tdc2/Oct neurons. These results were independently substantiated using the conditional *Tdc2-LexA* driver *B3RT-Tdc2* that allows assessment of intersectional expression between any Gal4 driver and *Tdc2* neurons. While it

is possible that OctR distribution in Oct neurons is not presynaptic, results from vertebrates suggest autoreceptor modulation is likely (Cragg & Greenfield, 1997; Starke, 2001; Trendelenburg et al., 2003), even in dual neurotransmitter neurons (Takacs et al., 2018).

In the case of autoreception, the released neurotransmitter may activate the autoreceptor to regulate secretion of that same transmitter by either inhibiting or facilitating its release. Thus, autoreception brings a key regulatory aspect to neurotransmitter signaling that significantly impacts synaptic transmission, circuit output, and behavior (Choi et al., 2012; Koon et al., 2011; Koon & Budnik, 2012; Langer, 2015). In *Drosophila*, receptors for the neuropeptide peptide dispersing factor (PDF) are expressed in and required by PDF-expressing lateral ventral pacemaker neurons (LNv's) to shift the balance of activity from evening to morning (Choi et al., 2012). Serotonin regulates neurite outgrowth in an autocrine manner in Helisoma (Diefenbach, Sloley, & Goldberg, 1995) and in the ventral nerve cord of *Drosophila* larvae (Sykes & Condron, 2005). At the *Drosophila* NMJ, the growth of Oct arbors during development and in response to starvation requires the activation of Octβ2R autoreceptors, while the inhibition of synaptic growth depends on Octβ1R on presynaptic motorneurons (Koon et al., 2011; Koon & Budnik, 2012).

As Oct functions in such diverse capacities in invertebrates, the capability of an Oct neuron to presynaptically modulate its own release could have significant impacts on downstream circuit targets. For example, Tdc2+ neurons are required to promote aggression (Zhou, Rao, & Rao, 2008) and inhibit inter-male courtship (Andrews et al., 2014; Certel et al., 2010). Oct autoreceptors on these neurons may function to provide negative feedback to inhibit either aggression or courtship, depending on the social situation. While we investigated OctR expression in Oct neurons, the presence of other neurotransmitter receptors on Tdc2+ neurons may additionally affect computational output from these neurons, affecting a variety of systems in the fly. Our novel *B3RT-Tdc2* intersectional genetic tool allows future studies of other neurotransmitters or neurotransmitter receptors inputs in Tdc2+ neurons as it can be used in conjunction with any available Gal4 driver.

In such an investigation of Tdc2 expression with other neurotransmitters, we recently identified a subset of Tdc2+ neurons that also utilize glutamate (Sherer et al., in press). Glutamate is the major excitatory neurotransmitter at the *Drosophila* NMJ and glutamatergic neurons are found in all regions of the adult central brain (Daniels, Gelfand, Collins, & DiAntonio, 2008; Jan & Jan, 1976). In vertebrates, glutamate is co-released with dopamine, serotonin, acetylcholine, and GABA (Danik et al., 2005; Fattorini, Antonucci, Menna, Matteoli, & Conti, 2015; Ottem, Godwin, Krishnan, & Petersen, 2004; Wang et al., 2019). In *Drosophila*, glutamate enhances the efficiency of dopamine loading into synaptic vesicles (Aguilar et al., 2017).

Given recent results demonstrating Oct-glut co-expression (Sherer et al., in press), we investigated potential Oct and Glut postsynaptic receptor expression using the new Trojan-Gal4's. Similar to the conditional *Tdc2* driver created here, a conditional glutamate receptor driver, *KDRT-GluRIA*, was developed and used to reveal that *GluRIA* is co-expressed to a different degree with each *OctR-Gal4*. These results indicate these co-expressing neurons as putative postsynaptic targets of upstream dual Oct-Glut transmitting neurons (see Figure 13).

While we investigated *GluRIA* and *Tdc2* co-expression with OctRs, other neurotransmitters and neurotransmitter receptors are likely also co-expressed with Tdc2 (Croset et al., 2018), and future studies utilizing these new conditionally expressible genetic tools can expand our knowledge of octopaminergic dual transmitting signaling mechanisms.

Supplementary Material

Refer to Web version on PubMed Central for supplementary material.

ACKNOWLEDGMENTS

The authors thank the Bloomington Stock Center for fly lines and the Developmental Studies Hybridoma Bank for antibodies. NIH R01 GM115510 grant to S.J.C. and R.S.S. supported this work.

Funding information

NIH Center for Scientific Review, Grant/Award Number: R01 GM115510

REFERENCES

Aguilar JI, Dunn M, Mingote S, Karam CS, Farino ZJ, Sonders MS, … Freyberg Z. (2017). Neuronal depolarization drives increased dopamine synaptic vesicle loading via VGLUT. Neuron, 95(5), 1074–1088 e1077. 10.1016/j.neuron.2017.07.038

Andrews JC, Fernandez MP, Yu Q, Leary GP, Leung AK, Kavanaugh MP, … Certel SJ (2014). Octopamine neuromodulation regulates Gr32a-linked aggression and courtship pathways in drosophila males. PLoS Genetics, 10(5), e1004356. 10.1371/journal.pgen.1004356

Balfanz S, Strunker T, Frings S, & Baumann A. (2005). A family of octopamine [corrected] receptors that specifically induce cyclic AMP production or Ca2+ release in Drosophila melanogaster. Journal of Neurochemistry, 93(2), 440–451. 10.1111/j.1471-4159.2005.03034.x [PubMed: 15816867]

Busch S, Selcho M, Ito K, & Tanimoto H. (2009). A map of octopaminergic neurons in the Drosophila brain. The Journal of Comparative Neurology, 513(6), 643–667. 10.1002/cne.21966 [PubMed: 19235225]

Certel SJ, Leung A, Lin CY, Perez P, Chiang AS, & Kravitz EA (2010). Octopamine neuromodulatory effects on a social behavior decision-making network in drosophila males. PLoS One, 5(10), e13248. 10.1371/journal.pone.0013248

Certel SJ, & Thor S. (2004). Specification of drosophila motoneuron identity by the combinatorial action of POU and LIM-HD factors. Development, 131(21), 5429–5439. 10.1242/dev.01418 [PubMed: 15469973]

Choi C, Cao G, Tanenhaus AK, McCarthy EV, Jung M, Schleyer W, … Nitabach MN (2012). Autoreceptor control of peptide/neurotransmitter corelease from PDF neurons determines allocation of circadian activity in drosophila. Cell Reports, 2(2), 332–344. 10.1016/j.celrep.2012.06.021 [PubMed: 22938867]

Ciccarelli M, Sorriento D, Coscioni E, Iaccarino G, & Santulli G. (2016). Adrenergic receptors. In Endocrinology of the heart in health and disease (pp. 285–315). Elsevier.

Cole SH, Carney GE, McClung CA, Willard SS, Taylor BJ, & Hirsh J. (2005). Two functional but noncomplementing drosophila tyrosine decarboxylase genes: Distinct roles for neural tyramine and octopamine in female fertility. The Journal of Biological Chemistry, 280 (15), 14948–14955. 10.1074/jbc.M414197200

Cole SW, & Sood AK (2012). Molecular pathways: Beta-adrenergic signaling in cancer. Clinical Cancer Research, 18(5), 1201–1206. 10.1158/1078-0432.CCR-11-0641 [PubMed: 22186256]

Cragg SJ, & Greenfield SA (1997). Differential autoreceptor control of somatodendritic and axon terminal dopamine release in substantia nigra, ventral tegmental area, and striatum. Journal of Neuroscience, 17 (15), 5738–5746 Retrieved from https://www.ncbi.nlm.nih.gov/pubmed/9221772 [PubMed: 9221772]

Croset V, Treiber CD, & Waddell S. (2018). Cellular diversity in the drosophila midbrain revealed by single-cell transcriptomics. Elife, 7, e34550. 10.7554/eLife.34550

Daniels RW, Gelfand MV, Collins CA, & DiAntonio A. (2008). Visualizing glutamatergic cell bodies and synapses in drosophila larval and adult CNS. The Journal of Comparative Neurology, 508(1), 131–152. 10.1002/cne.21670 [PubMed: 18302156]

Danik M, Cassoly E, Manseau F, Sotty F, Mouginot D, & Williams S. (2005). Frequent coexpression of the vesicular glutamate transporter 1 and 2 genes, as well as coexpression with genes for choline acetyltransferase or glutamic acid decarboxylase in neurons of rat brain. Journal of Neuroscience Research, 81(4), 506–521. 10.1002/jnr.20500 [PubMed: 15983996]

Diao F, Ironfield H, Luan H, Diao F, Shropshire WC, Ewer J, … White BH (2015). Plug-and-play genetic access to drosophila cell types using exchangeable exon cassettes. Cell Reports, 10(8), 1410–1421. 10.1016/j.celrep.2015.01.059 [PubMed: 25732830]

Diefenbach TJ, Sloley BD, & Goldberg JI (1995). Neurite branch development of an identified serotonergic neuron from embryonic Helisoma: Evidence for autoregulation by serotonin. Developmental Biology, 167(1), 282–293. 10.1006/dbio.1995.1023 [PubMed: 7851649]

El-Kholy S, Stephano F, Li Y, Bhandari A, Fink C, & Roeder T. (2015). Expression analysis of octopamine and tyramine receptors in drosophila. Cell and Tissue Research, 361(3), 669–684. 10.1007/s00441-015-2137-4 [PubMed: 25743690]

Evans PD, & Maqueira B. (2005). Insect octopamine receptors: A new classification scheme based on studies of cloned drosophila G-protein coupled receptors. Invertebrate Neuroscience, 5(3–4), 111–118. 10.1007/s10158-005-0001-z [PubMed: 16211376]

Fattorini G, Antonucci F, Menna E, Matteoli M, & Conti F. (2015). Co-expression of VGLUT1 and VGAT sustains glutamate and GABA co-release and is regulated by activity in cortical neurons. Journal of Cell Science, 128(9), 1669–1673. 10.1242/jcs.164210 [PubMed: 25749864]

Han KA, Millar NS, & Davis RL (1998). A novel octopamine receptor with preferential expression in drosophila mushroom bodies. Journal of Neuroscience, 18(10), 3650–3658 Retrieved from https://www.ncbi.nlm.nih.gov/pubmed/9570796 [PubMed: 9570796]

Hnasko TS, & Edwards RH (2012). Neurotransmitter corelease: Mechanism and physiological role. Annual Review of Physiology, 74, 225–243. 10.1146/annurev-physiol-020911-153315

Hoopfer ED (2016). Neural control of aggression in drosophila. Current Opinion in Neurobiology, 38, 109–118. 10.1016/j.conb.2016.04.007 [PubMed: 27179788]

Jan LY, & Jan YN (1976). L-glutamate as an excitatory transmitter at the drosophila larval neuromuscular junction. The Journal of Physiology, 262(1), 215–236. 10.1113/jphysiol.1976.sp011593 [PubMed: 186587]

Klagges BR, Heimbeck G, Godenschwege TA, Hofbauer A, Pflugfelder GO, Reifegerste R, … Buchner E. (1996). Invertebrate synapsins: A single gene codes for several isoforms in drosophila. Journal of Neuroscience, 16(10), 3154–3165 Retrieved from https://www.ncbi.nlm.nih.gov/pubmed/8627354 [PubMed: 8627354]

Koon AC, Ashley J, Barria R, DasGupta S, Brain R, Waddell S, … Budnik V. (2011). Autoregulatory and paracrine control of synaptic and behavioral plasticity by octopaminergic signaling. Nature Neuroscience, 14(2), 190–199. 10.1038/nn.2716 [PubMed: 21186359]

Koon AC, & Budnik V. (2012). Inhibitory control of synaptic and behavioral plasticity by octopaminergic signaling. The Journal of Neuroscience, 32(18), 6312–6322. 10.1523/JNEUROSCI.6517-11.2012 [PubMed: 22553037]

Langer SZ (2015). alpha2-Adrenoceptors in the treatment of major neuropsychiatric disorders. Trends in Pharmacological Sciences, 36(4), 196–202. 10.1016/j.tips.2015.02.006 [PubMed: 25771972]

Langer SZ, & Angel I. (1991). Pre- and postsynaptic alpha-2 adrenoceptors as target for drug discovery. Journal of Neural Transmission. Supplementum, 34, 171–177. 10.1007/978-3-7091-9175-0_22 [PubMed: 1687782]

Li-Kroeger D, Kanca O, Lee PT, Cowan S, Lee MT, Jaiswal M, … Bellen HJ (2018). An expanded toolkit for gene tagging based on MiMIC and scarless CRISPR tagging in drosophila. Elife, 7, e38709. 10.7554/eLife.38709

Maqueira B, Chatwin H, & Evans PD (2005). Identification and characterization of a novel family of Drosophila beta-adrenergic-like octopamine G-protein coupled receptors. Journal of Neurochemistry, 94(2), 547–560. 10.1111/j.1471-4159.2005.03251.x [PubMed: 15998303]

Meiselman MR, Kingan TG, & Adams ME (2018). Stress-induced reproductive arrest in drosophila occurs through ETH deficiency-mediated suppression of oogenesis and ovulation. BMC Biology, 16(1), 18. 10.1186/s12915-018-0484-9 [PubMed: 29382341]

Monastirioti M. (2003). Distinct octopamine cell population residing in the CNS abdominal ganglion controls ovulation in Drosophila melanogaster. Developmental Biology, 264(1), 38–49. 10.1016/j.ydbio.2003.07.019 [PubMed: 14623230]

Nassel DR (2018). Substrates for neuronal Cotransmission with neuropeptides and small molecule neurotransmitters in drosophila. Frontiers in Cellular Neuroscience, 12, 83. 10.3389/fncel.2018.00083 [PubMed: 29651236]

Nern A, Pfeiffer BD, Svoboda K, & Rubin GM (2011). Multiple new site-specific recombinases for use in manipulating animal genomes. Proceedings of the National Academy of Sciences of the United States of America, 108(34), 14198–14203. 10.1073/pnas.1111704108

Ottem EN, Godwin JG, Krishnan S, & Petersen SL (2004). Dualphenotype GABA/glutamate neurons in adult preoptic area: Sexual dimorphism and function. The Journal of Neuroscience, 24(37), 8097–8105. 10.1523/JNEUROSCI.2267-04.2004 [PubMed: 15371511]

Pauls D, Blechschmidt C, Frantzmann F, El Jundi B, & Selcho M. (2018). A comprehensive anatomical map of the peripheral octopaminergic/tyraminergic system of Drosophila melanogaster. Scientific Reports, 8(1), 15314. 10.1038/s41598-018-33686-3

Pech U, Pooryasin A, Birman S, & Fiala A. (2013). Localization of the contacts between Kenyon cells and aminergic neurons in the Drosophila melanogaster brain using SplitGFP reconstitution. The Journal of Comparative Neurology, 521(17), 3992–4026. 10.1002/cne.23388 [PubMed: 23784863]

Petersen LK, & Stowers RS (2011). A gateway MultiSite recombination cloning toolkit. PLoS One, 6(9), e24531. 10.1371/journal.pone.0024531

Pfeiffer BD, Jenett A, Hammonds AS, Ngo TT, Misra S, Murphy C, … Rubin GM (2008). Tools for neuroanatomy and neurogenetics in drosophila. Proceedings of the National Academy of Sciences of the United States of America, 105(28), 9715–9720. 10.1073/pnas.0803697105 [PubMed: 18621688]

Pittaluga A. (2016). Presynaptic release-regulating mGlu1 receptors in central nervous system. Frontiers in Pharmacology, 7, 295. 10.3389/fphar.2016.00295 [PubMed: 27630571]

Port F, Chen HM, Lee T, & Bullock SL (2014). Optimized CRISPR/Cas tools for efficient germline and somatic genome engineering in drosophila. Proceedings of the National Academy of Sciences of the United States of America, 111(29), E2967–E2976. 10.1073/pnas.1405500111

Qi YX, Xu G, Gu GX, Mao F, Ye GY, Liu W, & Huang J. (2017). A new drosophila octopamine receptor responds to serotonin. Insect Biochemistry and Molecular Biology, 90, 61–70. 10.1016/j.ibmb.2017.09.010 [PubMed: 28942992]

Ren X, Sun J, Housden BE, Hu Y, Roesel C, Lin S, … Ni JQ (2013). Optimized gene editing technology for Drosophila melanogaster using germ line-specific Cas9. Proceedings of the National Academy of Sciences of the United States of America, 110(47), 19012–19017. 10.1073/pnas.1318481110

Riabinina O, & Potter CJ (2016). The Q-system: A versatile expression system for drosophila. Methods in Molecular Biology, 1478, 53–78. 10.1007/978-1-4939-6371-3_3 [PubMed: 27730575]

Roeder T. (1999). Octopamine in invertebrates. Progress in Neurobiology, 59(5), 533–561 Retrieved from https://www.ncbi.nlm.nih.gov/pubmed/10515667 [PubMed: 10515667]

Sallee F, Connor DF, & Newcorn JH (2013). A review of the rationale and clinical utilization of alpha2-adrenoceptor agonists for the treatment of attention-deficit/hyperactivity and related disorders. Journal of Child and Adolescent Psychopharmacology, 23(5), 308–319. 10.1089/cap.2013.0028 [PubMed: 23782125]

Santulli G, & Iaccarino G. (2013). Pinpointing beta adrenergic receptor in ageing pathophysiology: Victim or executioner? Evidence from crime scenes. Immunity & Ageing, 10(1), 10. 10.1186/17424933-10-10 [PubMed: 23497413]

Seal RP, & Edwards RH (2006). Functional implications of neurotransmitter co-release: Glutamate and GABA share the load. Current Opinion in Pharmacology, 6(1), 114–119. 10.1016/j.coph.2005.12.001 [PubMed: 16359920]

Sherer LM, Catudio-Garrett E, Morgan HR, Sirrs LA, Shearin HK, Williams JL, … Certel SJ (2020). Octopamine-dependent aggression requires dVGLUT from dual-transmitting neurons. PLoS Genetics, [Epub ahead of print]

Snyder A, & Silberman Y. (2019). Stress engages novel beta-adrenergic receptor and CRF1 receptor mediated glutamatergic signaling in the ventral bed nucleus of the stria terminalis. The FASEB Journal, 33 (1_Suppl), 850.816. 10.1096/fasebj.2019.33.1_supplement.850.16

Starke K. (2001). Presynaptic autoreceptors in the third decade: Focus on alpha2-adrenoceptors. Journal of Neurochemistry, 78(4), 685–693. 10.1046/j.1471-4159.2001.00484.x [PubMed: 11520889]

Sykes PA, & Condron BG (2005). Development and sensitivity to serotonin of drosophila serotonergic varicosities in the central nervous system. Developmental Biology, 286(1), 207–216. 10.1016/j.ydbio.2005.07.025 [PubMed: 16122730]

Takacs VT, Cserep C, Schlingloff D, Posfai B, Szonyi A, Sos KE, … Nyiri G. (2018). Co-transmission of acetylcholine and GABA regulates hippocampal states. Nature Communications, 9(1), 2848. 10.1038/s41467-018-05136-1

Trendelenburg AU, Philipp M, Meyer A, Klebroff W, Hein L, & Starke K. (2003). All three alpha2-adrenoceptor types serve as autoreceptors in postganglionic sympathetic neurons. NaunynSchmiedeberg's Archives of Pharmacology, 368(6), 504–512. 10.1007/s00210-003-0829-x [PubMed: 14610637]

Ultsch A, Schuster CM, Laube B, Schloss P, Schmitt B, & Betz H. (1992). Glutamate receptors of Drosophila melanogaster: Cloning of a kainate-selective subunit expressed in the central nervous system. Proceedings of the National Academy of Sciences of the United States of America, 89(21), 10484–10488. 10.1073/pnas.89.21.10484

Vaaga CE, Borisovska M, & Westbrook GL (2014). Dual-transmitter neurons: Functional implications of co-release and co-transmission. Current Opinion in Neurobiology, 29, 25–32. 10.1016/j.conb.2014.04.010 [PubMed: 24816154]

Vaniotis G, Del Duca D, Trieu P, Rohlicek CV, Hebert TE, & Allen BG (2011). Nuclear beta-adrenergic receptors modulate gene expression in adult rat heart. Cellular Signalling, 23(1), 89–98. 10.1016/j.cellsig.2010.08.007 [PubMed: 20732414]

Wang HL, Zhang S, Qi J, Wang H, Cachope R, Mejias-Aponte CA, … Morales M. (2019). Dorsal raphe dual serotonin-glutamate neurons drive reward by establishing excitatory synapses on VTA mesoaccumbens dopamine neurons. Cell Reports, 26(5), 1128–1142 e1127. 10.1016/j.celrep.2019.01.014

Zhou C, Rao Y, & Rao Y. (2008). A subset of octopaminergic neurons are important for drosophila aggression. Nature Neuroscience, 11(9), 1059–1067. 10.1038/nn.2164 [PubMed: 19160504]

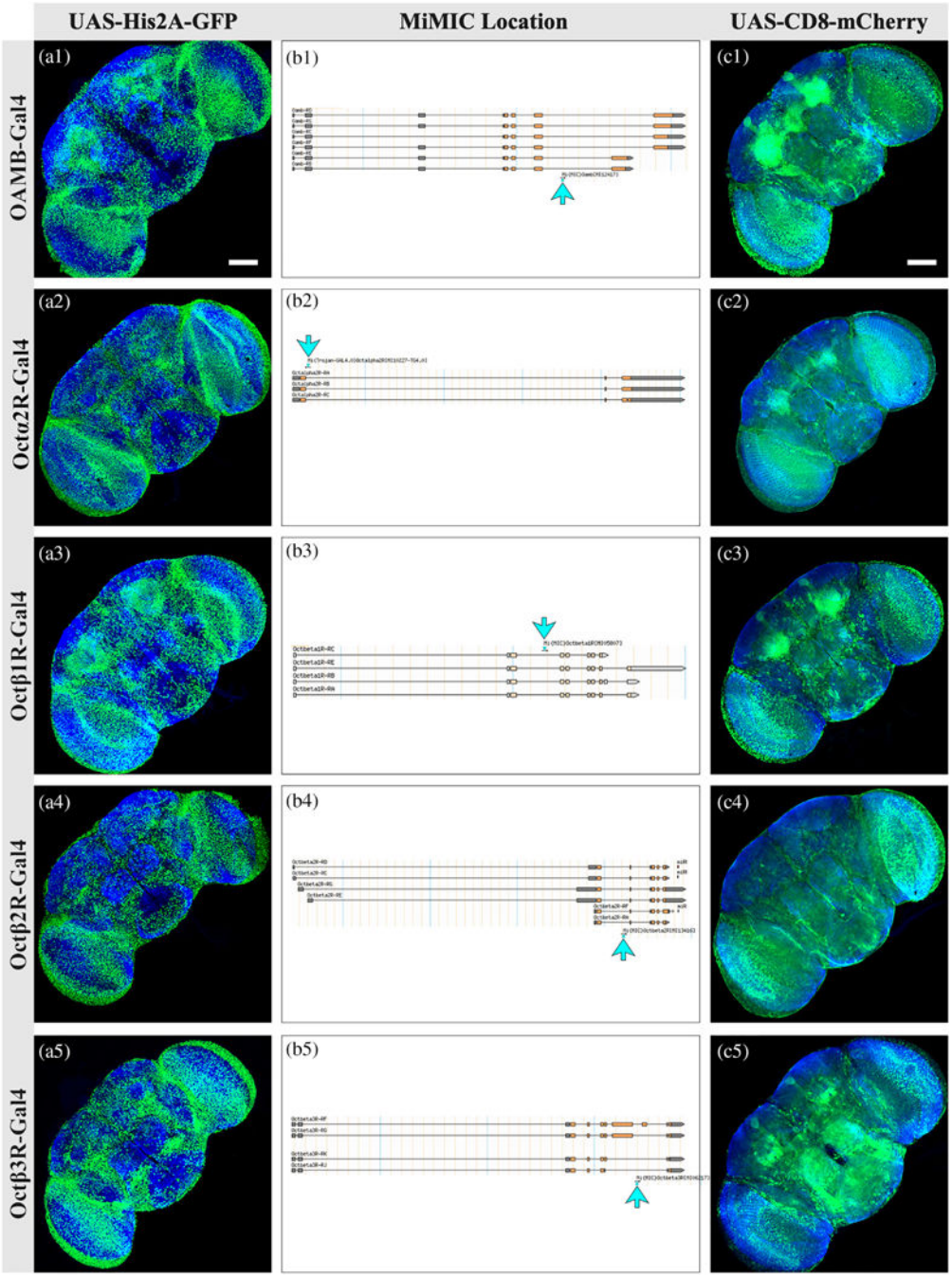

FIGURE 1.

Expression patterns of MiMIC *OctR-Gal4* lines. Nuclear expression patterns in male adult brains for (a1) *OAMB* > *His2A-GFP*, (a2) *Octα2R* > *His2A-GFP*, (a3) *Octβ1R* > *His2A-GFP*, (a4) *Octβ2R* > *His2A-GFP*, (a5) *Octβ3R* > *His2A-GFP*; genomic locations of MiMIC insertions retrieved from flybase.org for (b1) *OAMB-Gal4*, (b2) *Octα2R*, (b3) *Octβ1R*, (b4) *Octβ2R*, (b5) *Octβ3R*; expression patterns using a plasma membrane reporter (c1) *OAMB* > *CD8-mCherry*, (c2) *Octα2R* > *CD8-mCherry*, (c3) *Octβ1R* > *CD8-mCherry*, (c4) *Octβ2R* >

CD8-mCherry, (c5) *Octβ3R* > *CD8-mCherry*. Scale bar = 75 μm. Antibodies used: anti-mCherry (green) and anti-SYN (blue)

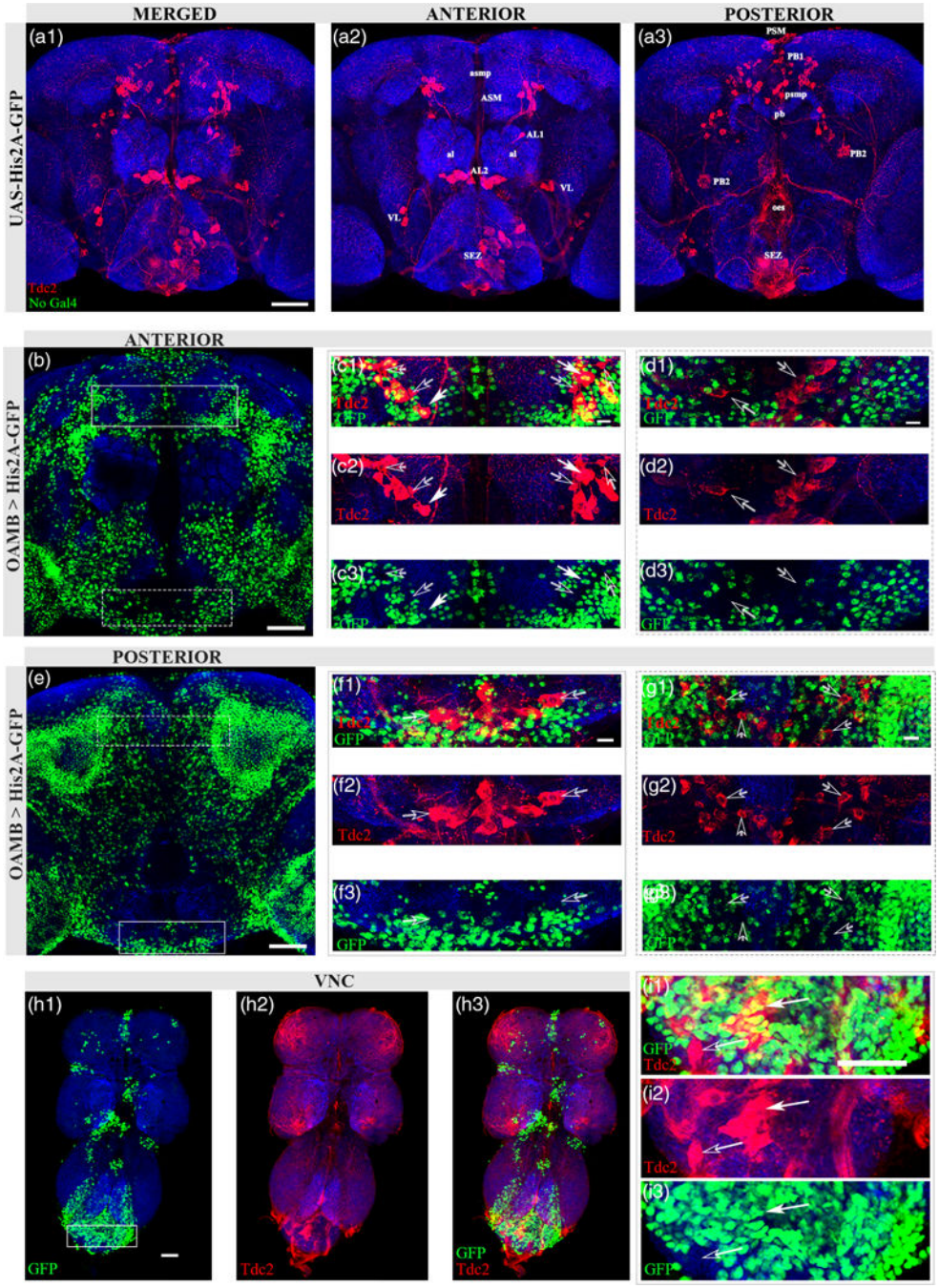

FIGURE 2.

OAMB is expressed in a subset of Oct neurons. (a1) Tdc2 expression (red) in a control *UAS-His2A-GFP*/+ brain. Scale bar = 50 μm (a2) Anterior optical sections of (a1) outlining Tdc2+ neuronal clusters (uppercase): ASM cluster in the ASMP (anterior superior medial protocerebrum), AL (antennal lobe) clusters AL1 and AL2, VL (ventrolateral), SEZ (subesophageal ganglion) (a3) Posterior sections of (a1): PSM and PB1 clusters in posterior superior medial protocerebrum (PSMP), PB2 cluster in pb (protocerebral bridge), oes (esophagus), SEZ (b) Anterior sections (46–76) of OAMB > His2A-GFP. Scale bar = 50 μm.

(c1–c3) Solid white rectangle from b showing co-expression of Tdc2 (red) and *OAMB* (green) in the ASM cluster of Tdc2 neurons (closed arrows) and neurons with no co-expression (open arrows). Scale bar = 10 μm. (d1–d3) Dashed rectangle from (b) showing no co-expressing neurons in the SEZ (open arrows) Scale bar = 10 μm. (e) Posterior sections (1–37) of *OAMB* > *His2A-GFP*. Scale bar = 50 μm. (f1–f3) Solid white rectangle from (e) showing no discernible co-expression in the SEZ (open arrows). (g) Dashed rectangle from (e) showing no co-expression seen in the PSMP region of the brain (open arrows). Scale bar = 10 μm. Antibodies used: anti-Tdc2 (red), anti-GFP (green), and anti-SYN (blue). (h1–h3) Nuclear GFP (h1, green) expression pattern in adult VNC with Tdc2 (h2, red) co-expression (h3, closed white arrow). Scale bar =30 μm. (i1–i3) Solid rectangle from (h1) showing neurons co-expressing with Tdc2 (closed white arrow) and neurons without Tdc2 co-expression (open white arrow) in the VNC. Scale bar = 30 μm. Antibodies used (h1–i3): anti-brp (blue), anti-GFP (green), anti-Tdc2 (red)

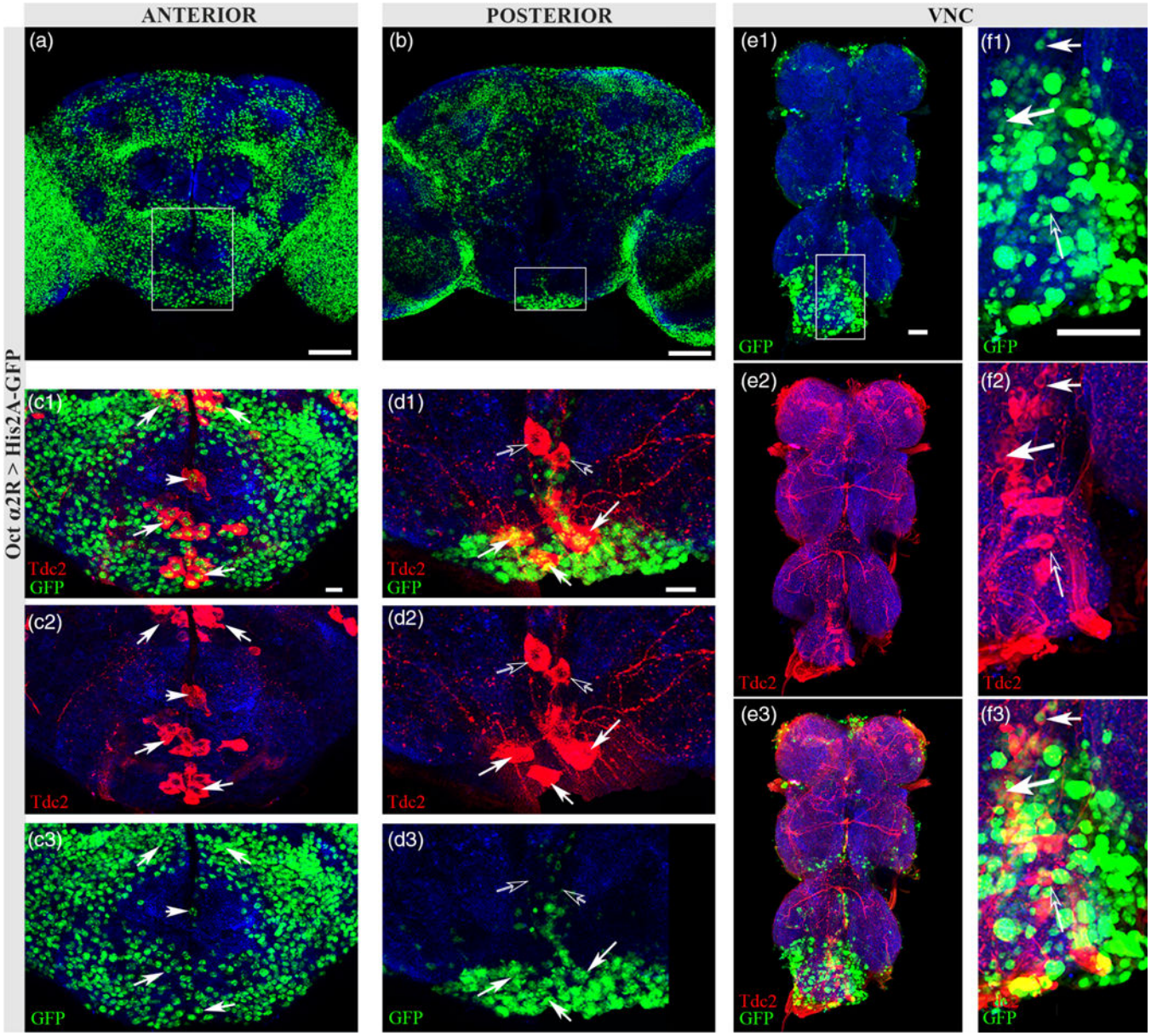

FIGURE 3.

Octα2R is expressed in a subset of Oct neurons. (a) Anterior optical sections (58–79) of *Octα2R* > *His2A-GFP*. Scale bar = 50 μm.(b) Posterior sections (3–37) of *Octα2R* > *His2A-GFP*. Scale bar = 50 μm. (c1–c3) Solid white rectangle from (a) showing co-expression of nuclear GFP (green) in Tdc2-stained somata (red) of the SEZ (closed arrows). Scale bar = 10 μm. (d1–d3) Solid white rectangle from (b) showing co-expression (closed arrows) of Tdc2 and nuclear GFP in posterior SEZ neurons. Open arrows indicate a single pair of SEZ neurons with no co-expression. Scale bar = 10 μm. Antibodies used: anti-GFP (green), anti-SYN (blue), anti-Tdc2 (red). (e1–e3) Nuclear GFP (e1, green) expression pattern in adult VNC with Tdc2 (e2, red) co-expression (e3, closed white arrows). Scale bar = 30 μm. (f1–f3) Solid rectangle from (e1) showing co-expression (closed white arrows) and at least one

neuron with no co-expression (open arrow) in the VNC. Scale bar = 30 μm. Antibodies used (e1–f3): anti-brp (blue), anti-GFP (green), and anti-Tdc2 (red)

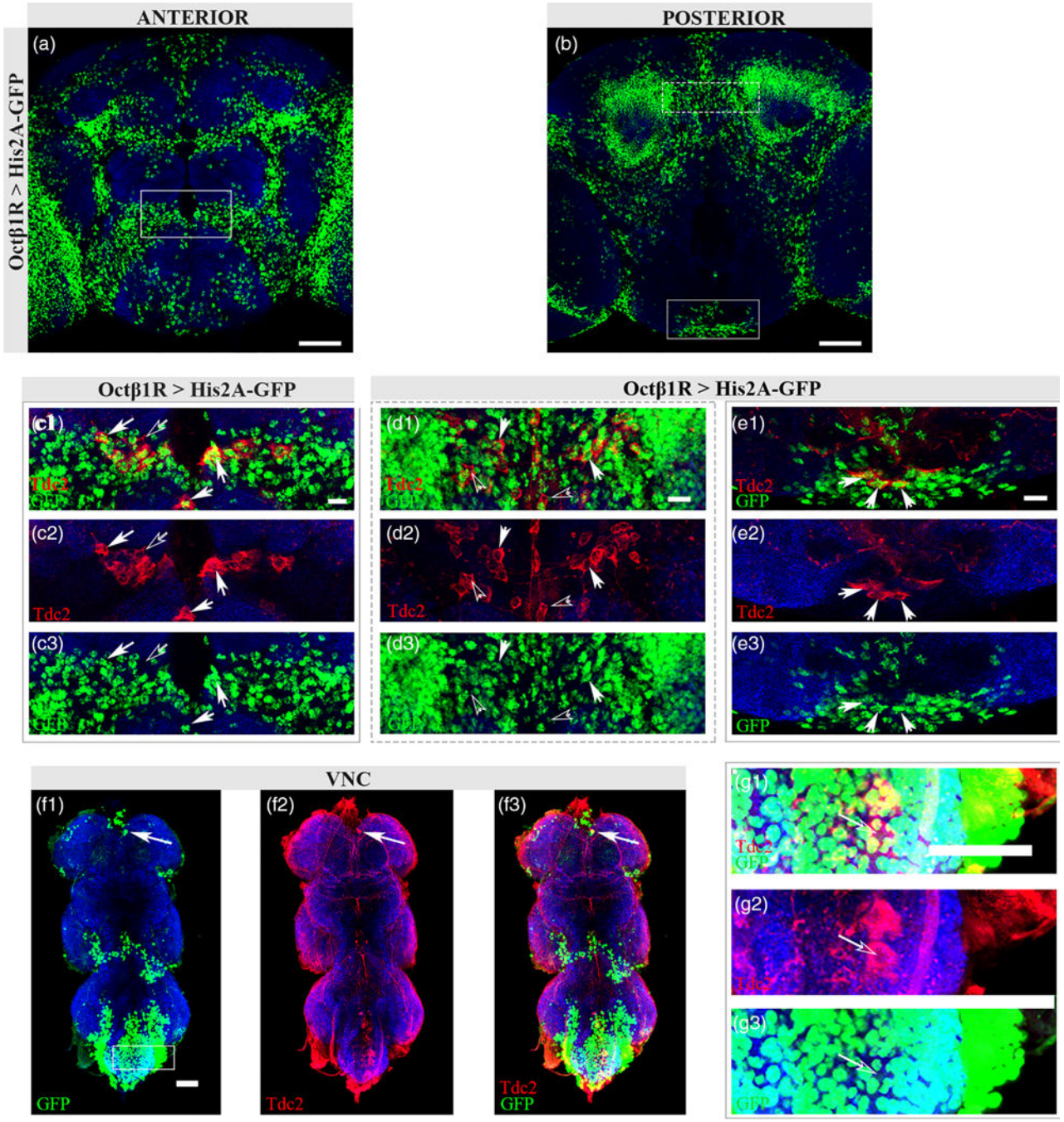

FIGURE 4.

Octβ1R is expressed in a subset of Oct neurons. (a) Anterior sections (26–33) of *Octβ1R* > *His2A-GFP* showing broad GFP expression. Scale bar = 50 μm. (b) Posterior sections (6–14) of *Octβ1R* > *His2A-GFP*. Scale bar = 50 μm. (c–c2) Solid white rectangle from (a) showing co-expression of *Octβ1R* > *His2A-GFP* (green) in the AL2 cluster Tdc2+ neurons (red). Scale bar = 10 μm. (d–d2) Dashed rectangle from (b) showing *Octβ1R* co-expression in the Tdc2+ (red) PB1 cluster (closed arrows). Neurons negative for co-expression are illustrated with open arrows. Scale bar = 10 μm. (e1–e3) Solid white rectangle from (b)

showing co-expression of *Octβ1R* > *His2A-GFP* (green) in Tdc2+ neurons (red) in posterior SEZ (closed arrows). Scale bar = 10 μm. Antibodies used: anti-GFP (green), anti-Tdc2 (red), anti-SYN (blue). (f1–f3) Nuclear GFP (f1, green) expression pattern in adult VNC with Tdc2 (f2, red) co-expression (f3, closed white arrow). Scale bar = 30 μm. (g1–g3) Solid rectangle from (f1) showing a neuron without co-expression with Tdc2 (open arrow). Scale bar =30 μm. Antibodies used (f1–g3): anti-brp (blue), anti-GFP (green), anti-Tdc2 (red)

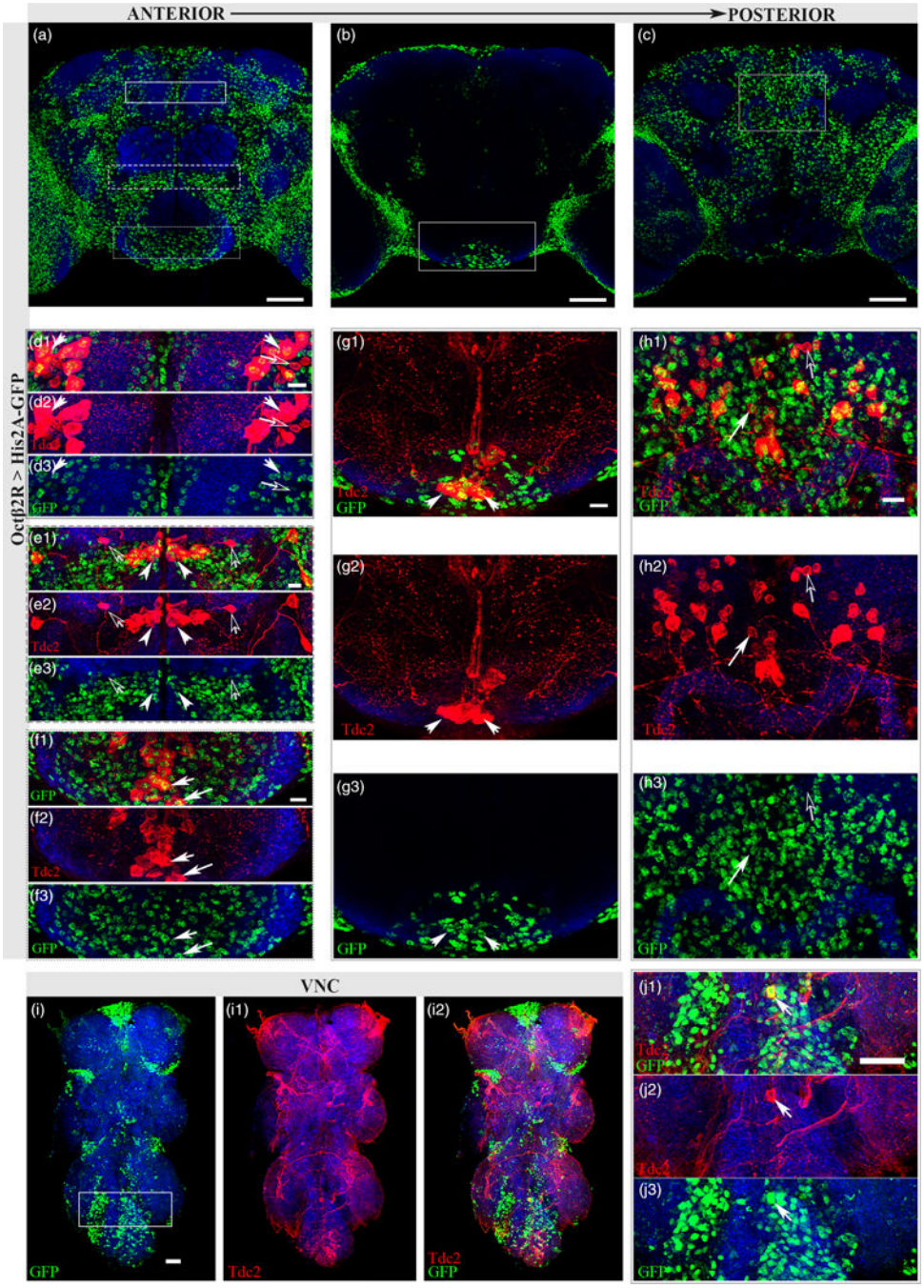

FIGURE 5.

Octβ2R expresses in a subset of Oct neurons. (a) Anterior sections (70–93) of *Octβ2R* > *His2A-GFP*. Scale bar = 50 μm. (b) Middle sections (36–65) of *Octβ2R* > *His2A-GFP*. Scale bar = 50 μm. (c) Posterior sections (15–31) of *Octβ2R* > *His2A-GFP*. Scale bar 50 μm. (d1–d3) Solid white rectangle from (a) showing co-expression of Tdc2 (red) and *Octβ2R* > *His2A-GFP*(green) in the ASM cluster (closed arrows) with at least one pair of Tdc2 neurons showing no co-expression (open arrows). Scale bar = 10 μm (e1–e3) Dashed rectangle from (a) indicating co-expression of Tdc2 (red) and *Octβ2R* > *His2A-GFP* (green)

in AL2 cluster (closed white arrows). A pair of AL1 neurons (open white arrows) did not exhibit co-expression. Scale bar = 10 μm. (f1–f3) Dotted rectangle from (a) showing co-expression in the anterior section of the SEZ (closed arrows). Scale bar = 10 μm (g1–g3) Solid white rectangle from (b) showing co-expression in the SEZ. Scale bar = 10 μm. (h1–h3) Some co-expression of Tdc2 and *Octβ2R* > *His2A-GFP* (closed arrows) and neurons not showing co-expression (open arrows) in the PB1 cluster of the PSMP region. Scale bar = 10 μm. Antibodies used: anti-Tdc2 (red), anti-GFP (green) and anti-SYN (blue). (i1–i3) Nuclear GFP (i1, green) expression pattern in adult VNC with Tdc2 (i2, red) co-expression in one neuron (i3). Scale bar = 30 μm. (j1–j3) Solid rectangle from (i1) with only one neuron showing co-expression with Tdc2 (closed white arrow). Scale bar = 30 μm. Antibodies used (f1–g3): anti-brp (blue), anti-GFP (green), anti-Tdc2 (red)

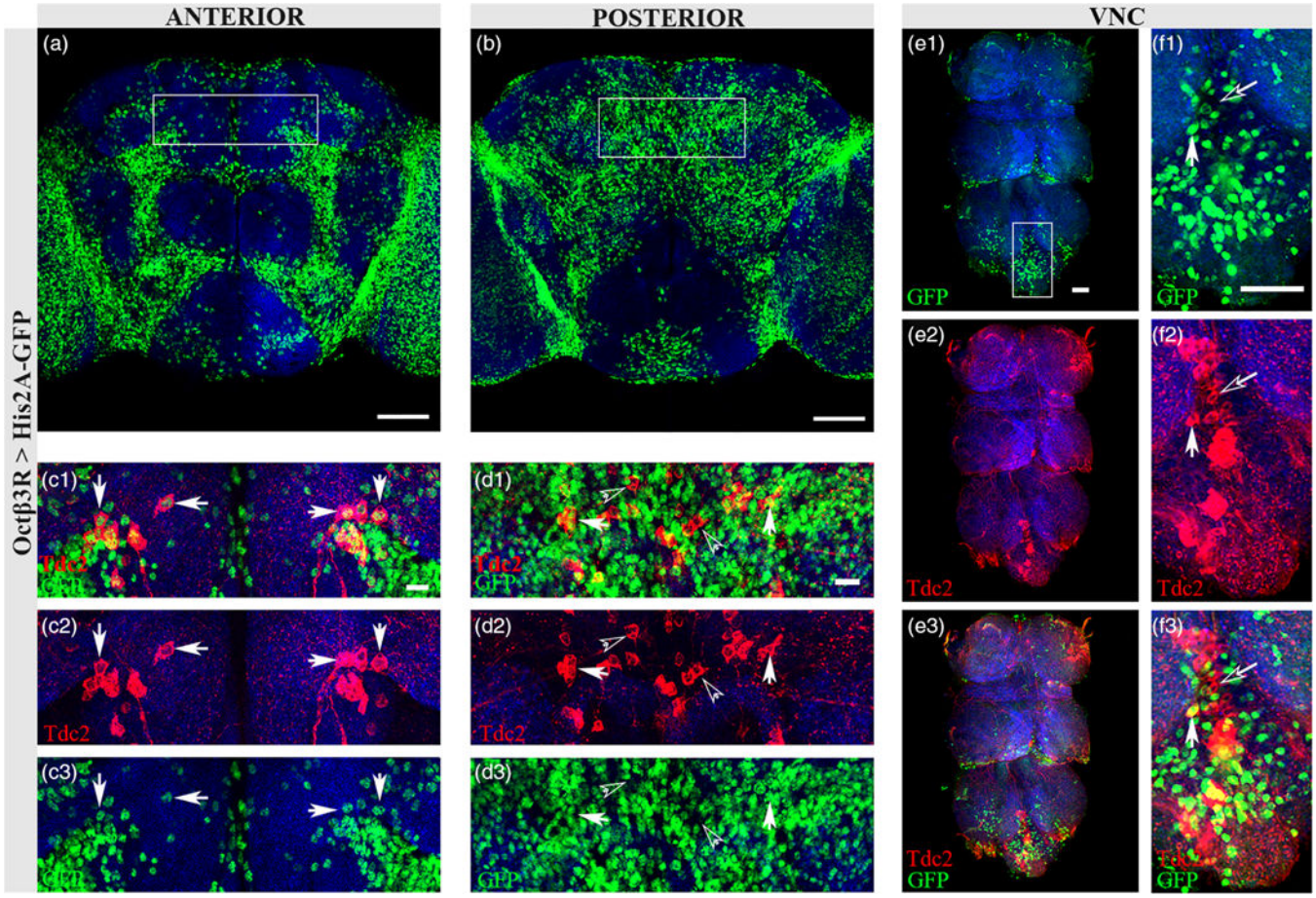

FIGURE 6.

Octβ3R is expressed in a subset of Oct neurons. (a) Anterior sections (32–42) of *Octβ3R* > *His2A-GFP*. Scale bar = 50 μm. (b) Posterior sections (0–26) of *Octβ3R* > *His2A-GFP*. Scale bar = 50 μm. (c1-c3) White rectangle from (a) showing co-expression in the ASM cluster of Tdc2 neurons (closed arrows). Scale bar = 10 μm. (d1–d3) White rectangle from (b) showing some co-expression in PSMP cluster of Tdc2 neurons (closed arrows) and some neurons negative for co-expression (open arrows). Scale bar 10 μm. Antibodies used: anti-Tdc2 (red), anti-GFP (green) and anti-SYN (blue). (e1–e3) Nuclear GFP (e1, green) expression pattern in adult VNC with Tdc2 (e2, red) co-expression (e3). Scale bar = 30 μm. (f1–f3) Solid rectangle from (e1) showing co-expression with Tdc2 (closed white arrow) and neurons showing no co-expression (open arrow). Scale bar = 30 μm. Antibodies used: anti-brp (blue), anti-GFP (green), anti-Tdc2 (red)

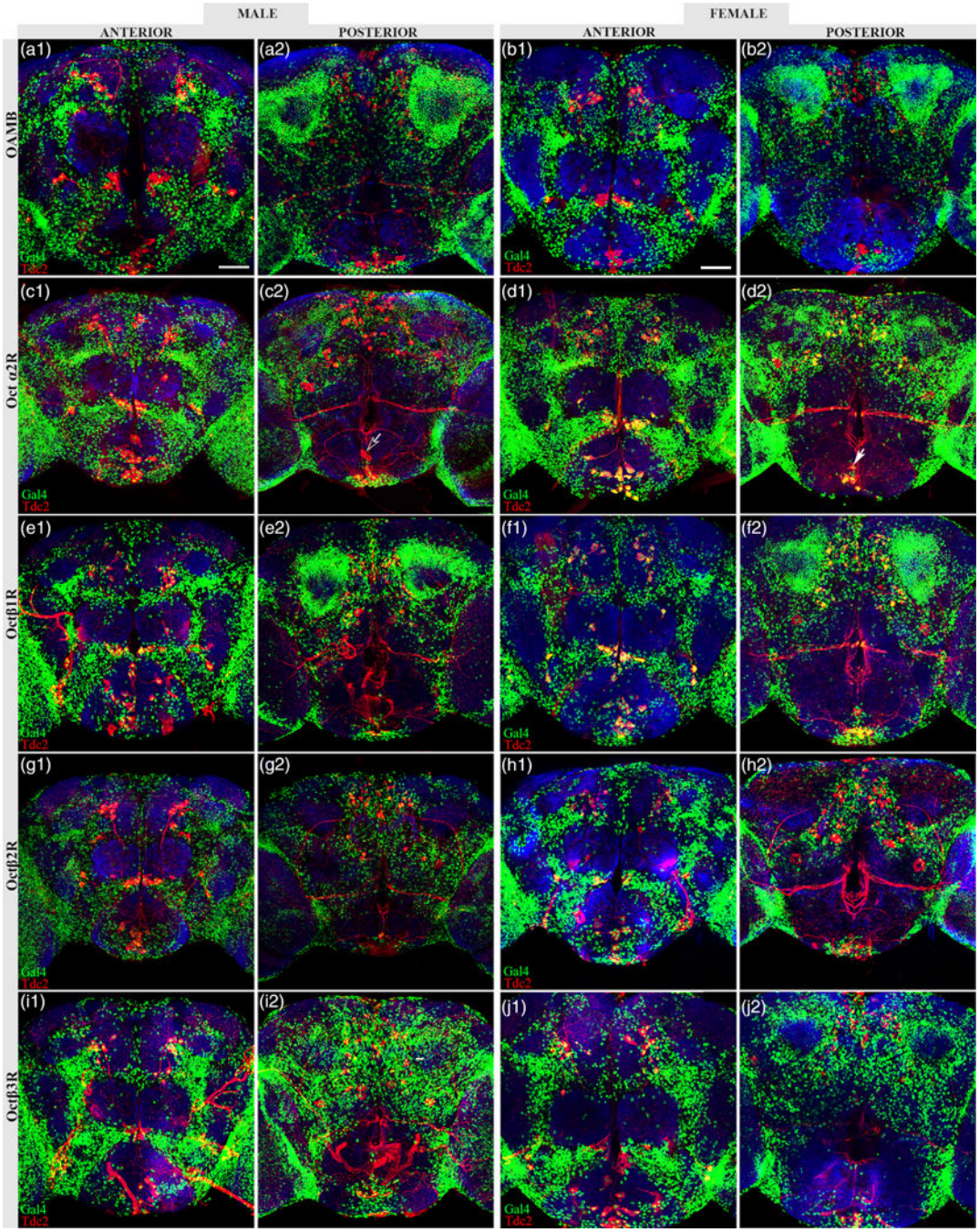

FIGURE 7.

Examination of sex differences among *OctR-Gal4* lines. Full z-stacks of anterior and posterior sections of male and female brains with overlapping Tdc2 stain. (a1–b2) *OAMB-Gal4 > His2A-GFP*, (c1–d2) *Octα2R-Gal4 > His2A-GFP*, (e1–f2) *Octβ1R-Gal4 > His2A-GFP*, (g1–h2) *Octβ2R-Gal4 > His2A-GFP*, and (i1–j2) *Octβ3R-Gal4 > His2A-GFP*. Scale bars = 50 μm. Antibodies used: anti-SYN (blue), anti-GFP (green), anti-Tdc2 (red)

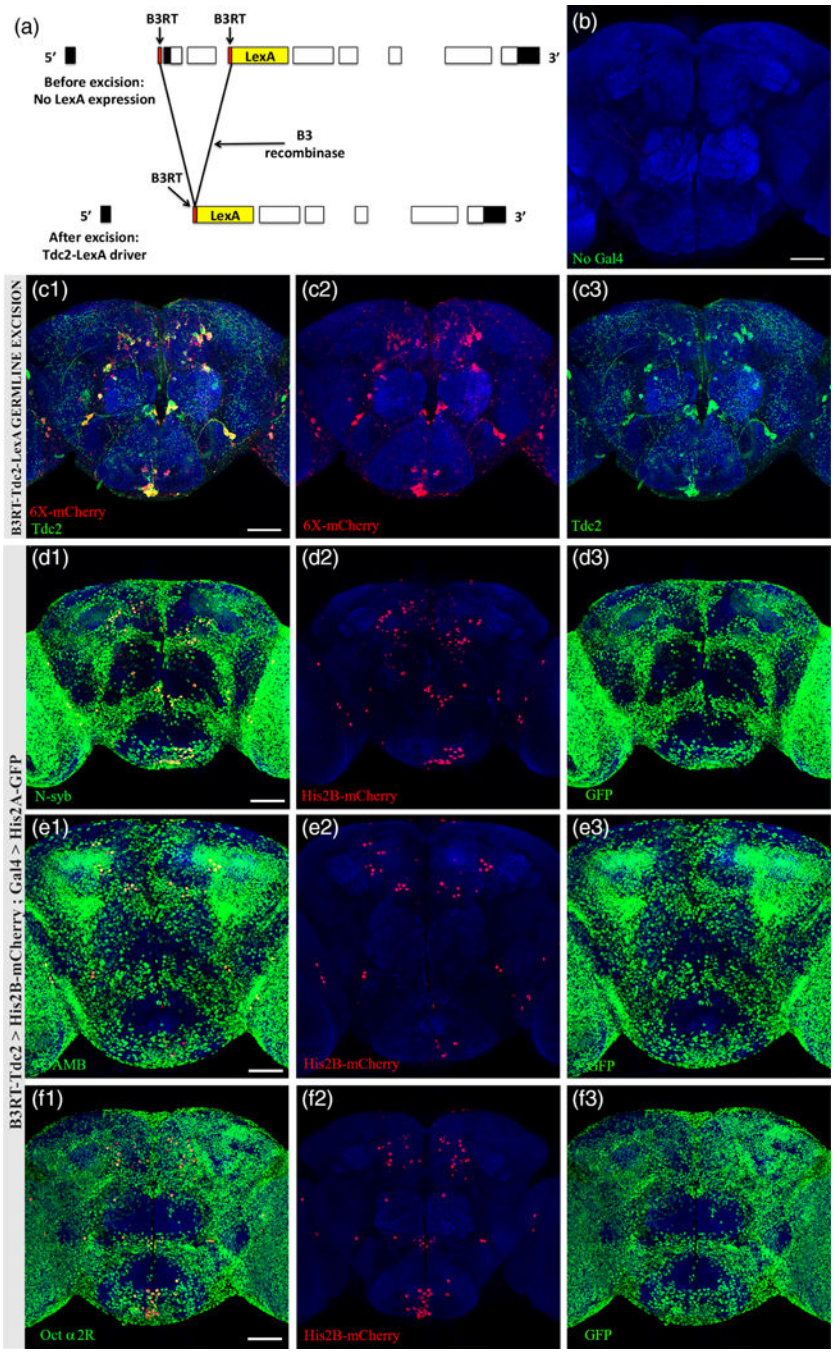

FIGURE 8.

B3RT-Tdc2 expression in α-adrenergic-like receptors. (a) Schematic of *B3RT-Tdc2-LexA*. CRISPR/Cas9 genome editing was used to insert same orientation B3 recombinase target sites (B3RTs) into the 5′ untranslated region (UTR) of the *Tdc2* gene and into the intron between the first two *Tdc2* coding exons. The coding sequence of the LexA transcription factor was also inserted immediately adjacent to the downstream *B3RT*. The B3 recombinase mediates excision between the B3RT's in all neurons that express the B3 recombinase using a Gal4 driver and *UAS-B3*. After the excision, a *Tdc2-LexA* driver is

created and is expressed only in the subset of Gal4-expressing neurons that also express *Tdc2* and not in Gal4-expressing neurons that do not express *Tdc2*. Black rectangles are untranslated exons, white rectangles are coding exons, red rectangles are B3RTs, and yellow rectangles are coding LexA sequence. (b) Control *B3RT-Tdc2* with no Gal4 driver, anti-mCherry (red), anti-SYN (blue), anti-GFP (green). (c) Germline excision of *B3RT-Tdc2* (see Section 2), where *Tdc2-LexA* is expressed in all *Tdc2* neurons, anti-syn (blue), anti-mCherry (red), anti-Tdc2 (green). (d1–d3) Nuclear expression of *n-syb-Gal4* (d3, anti-GFP, green) and subset of *nsyb-Gal4* neurons that express *Tdc2* (d2, anti-mCherry, red), anti-SYN (blue) *yw; B3RT-Tdc2, nsyb-Gal4; LexAop2-His2B-mCherry, UAS-His2A-GFP*. (e1–e3) *OAMB > His2A-GFP* (e3, anti-GFP, green) and the subset of *OAMB-Gal4* neurons which express *Tdc2* (e2, anti-mCherry, red), anti-SYN (blue): yw; *B3RT-Tdc2; LexAop2-His2B-mCherry, UAS-His2A-GFP/OAMB-Gal4*. (f1–f3) *Octα2R > His2A-GFP* (f3, anti-GFP, green) and subset of *Octα2-Gal4* neurons which express *Tdc2* (f2, anti-mCherry, red), anti-SYN (blue): *yw; B3RT-Tdc2; LexAop2-His2B-mCherry, UAS-His2A-GFP/Oct2R-Gal4*. All scale bars 50 μm

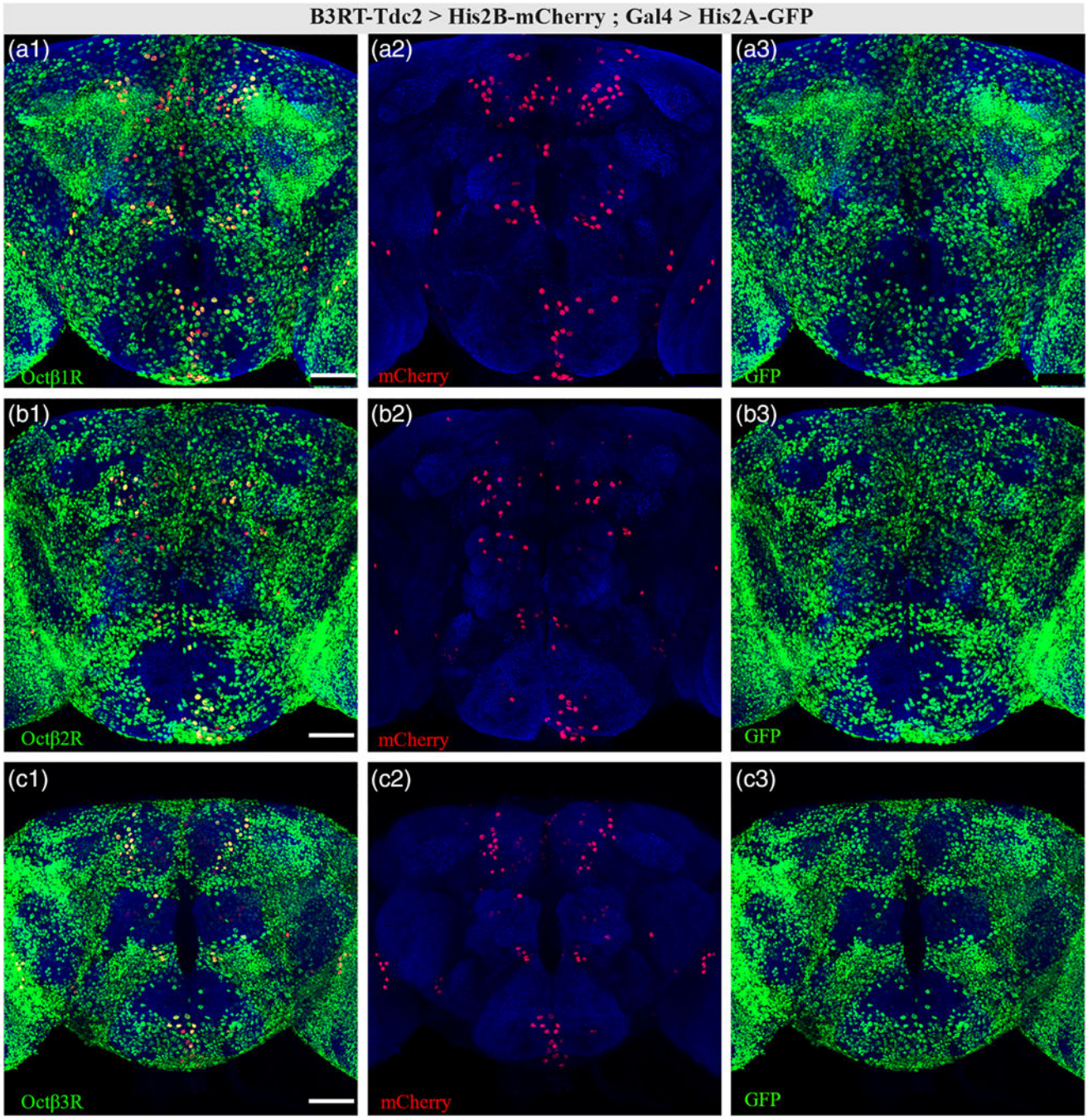

FIGURE 9.

B3RT-Tdc2 expression in *OctβR-Gal4s*. (a1–a3) *yw; B3RT-Tdc2; LexAop2-His2B-mCherry, UAS-His2A-GFP/Octβ1R-Gal4* showing subset of *Octβ1R-Gal4* neurons which also express *Tdc2* (a2, red), only the Gal4 pattern (a3, green) and merged (a1). (b1–b3) *yw; B3RT-Tdc2; LexAop2-His2B-mCherry, UAS-His2A-GFP/Octβ2R-Gal4* showing subset of *Octβ2R-Gal4* neurons that also express *Tdc2* (b2, red), only the Gal4 pattern (b3, green) and merged (b1). (c1–c3) *yw; B3RT-Tdc2; LexAop2-His2B-mCherry, UAS-His2A-GFP/ Octβ3R-Gal4* showing subset of *Octβ3R-Gal4* neurons that also express *Tdc2* (c2, red), only

the Gal4 pattern (c3, green) and merged (c1). Antibodies used: anti-GFP (green), anti-mCherry (red), and anti-SYN (blue). Scale bar = 50 μm

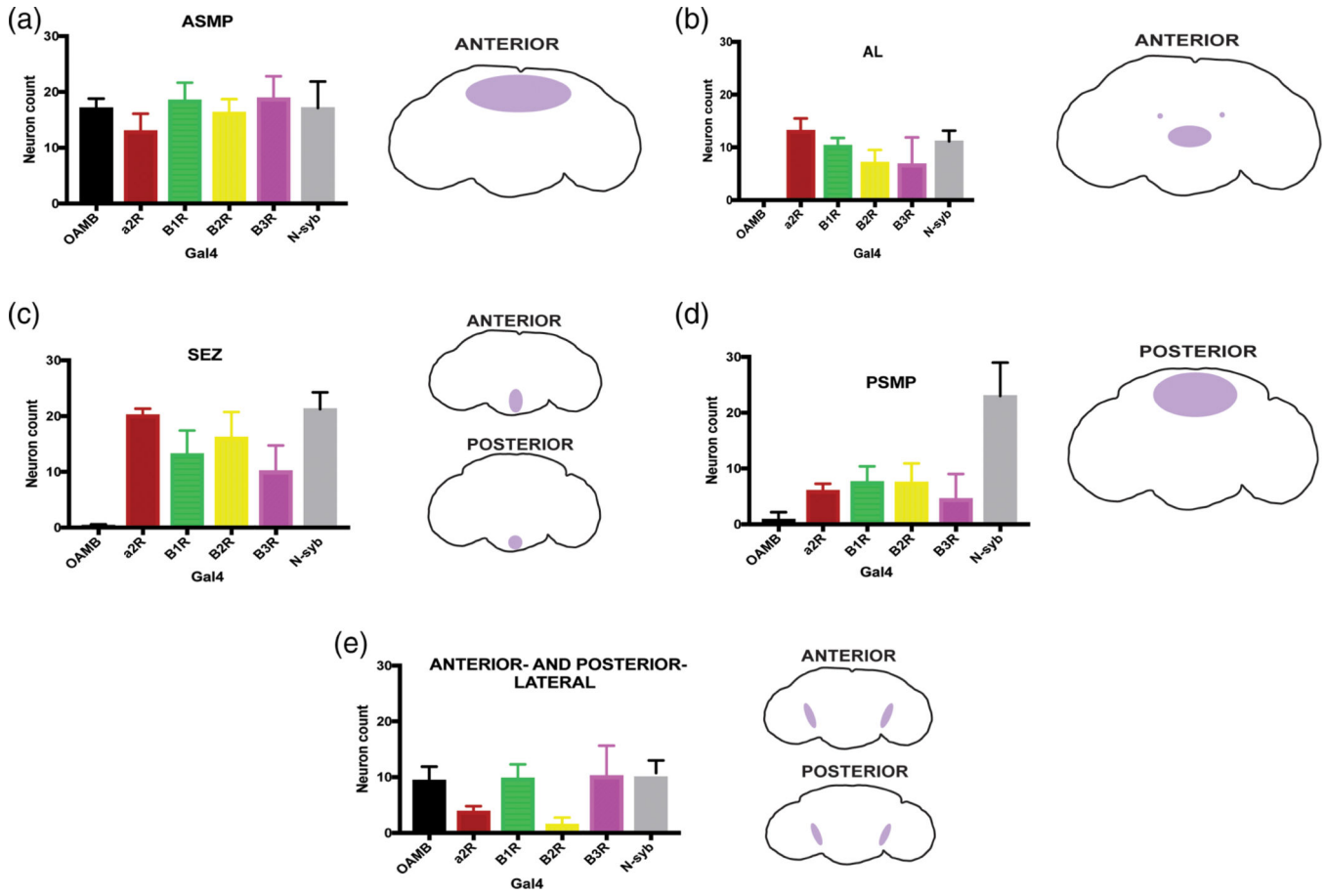

FIGURE 10.

Average number of co-expressing *OctR-Gal4|B3RT-Tdc2* neurons. Co-expressing *Gal4 > His2A-GFP|Tdc2-LexA > His2B-mCherry* neurons were manually counted in brain regions (a) anterior superior medial protocerebrum (ASMP), (b) antennal lobe (AL), (c) suboesophageal ganglion (SEZ), (d) posterior superior medial protocerebrum (PSMP), and (e) anterior- and posterior-lateral regions. *OAMB-Gal4* ($n = 12$), *Octα2R-Gal4* ($n = 6$), *Octβ1R-Gal4* ($n = 10$), *Octβ2R-Gal4* ($n = 10$), *Octβ3R-Gal4* ($n = 9$), *N-syb-Gal4* ($n = 8$)

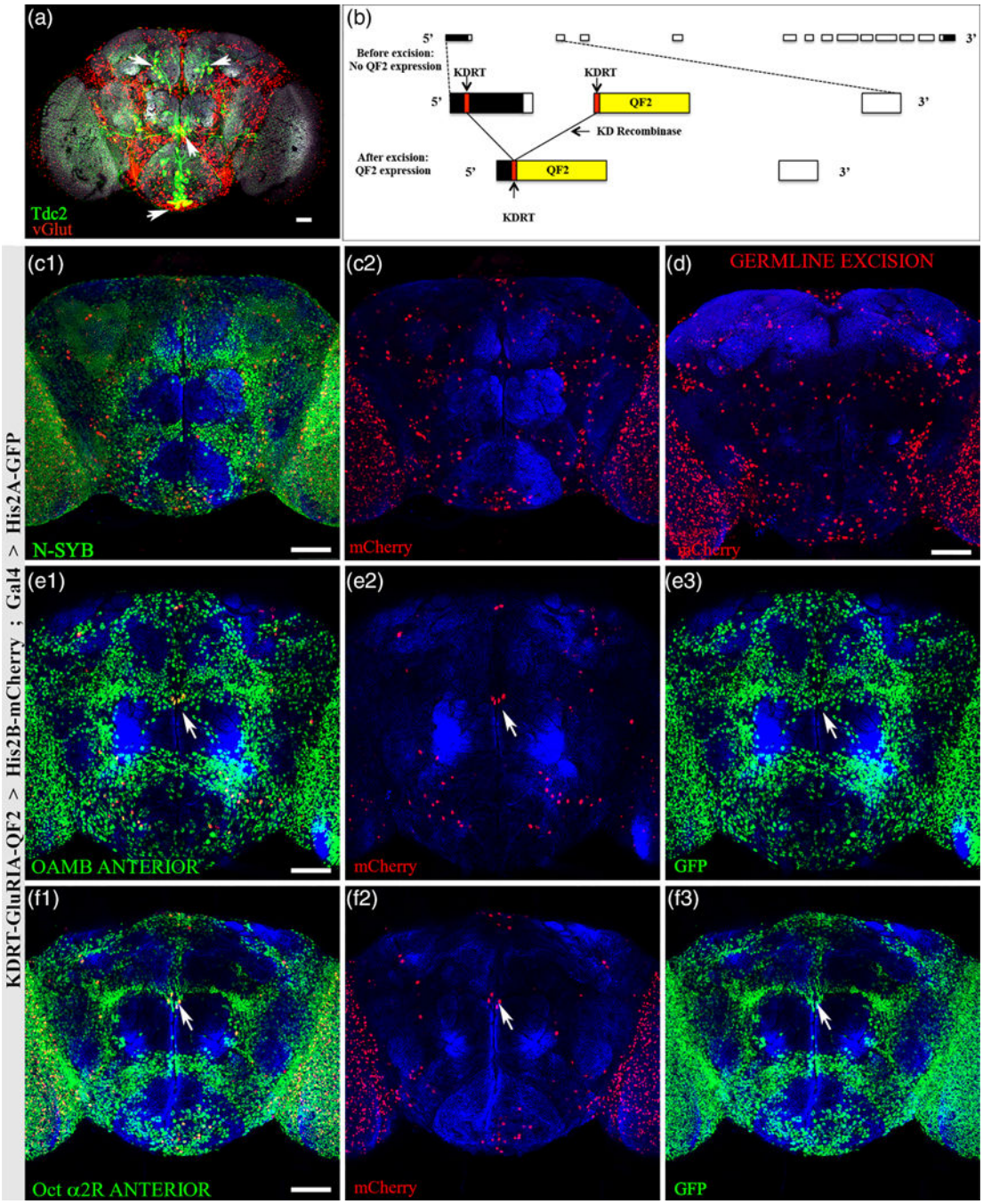

FIGURE 11.

KDRT-GluRIA expression in α-adrenergic-like receptors. (a) *vGlut-Gal4; UAS-dsRed* (red) and anti-Tdc2 (green) showing distinct co-localization, indicative of dual transmitting neurons (white arrows). Scale bar 30 μm. (b) Schematic of *KDRT-GluRIA-QF2* construct. The first KD recombination target site (*KDRT*) was CRISPR'd upstream of the endogenous locus of the *GluRIA* translation start site within the 5′ untranslated region (UTR) while the second *KDRT* was placed in an intron downstream of the translation start site, directly preceding a QF2 driver sequence. Prior to the excision of the DNA the two *KDRT*s flank, no

QF2 expression occurs. After the excision mediated by the KD recombinase, a null mutation in the *GluRIA* gene is formed, along with a *GluRIA-QF2* driver, which can drive the expression of our *QUAS* reporter of interest. (c1–c3) Pan-neuronal Gal4 driving expression of the KD recombinase in the subset of *n-syb-Gal4* neurons that express *GluRIA* (c2, red). *yw;n-syb-Gal4; KDRT-GluRIA, UAS-KD, UAS-His2A-GFP, QUAS-His2B-mCherry*. (d) Germline excision of *KDRT-GluRIA* driving expression of *QUAS-His2B-mCherry* in all *GluRIA*-expressing neurons (red). (e1–e3) *OAMB-His2A-GFP* pattern (e3, green), subset of *OAMB-Gal4* neurons expressing *GluRIA* (e2, red), and merged channels (e1) *yw; UAS-KD, UAS-His2A-GFP, QUAS-His2B-mCherry; KDRT-GluRIA, OAMB-Gal4*. Closed white arrow indicating four PENP neurons co-expressing *OAMB* and *GluRIA*. (f1–f3) *Octα2R > His2A-GFP* pattern (f3, green) and subset of *Octα2R-Gal4* neurons expressing *GluRIA* (f2, red), with broad expression seen in optic lobes. Merged channels (f1) *yw; UAS-KD, UAS-His2A-GFP, QUAS-His2B-mCherry; KDRT-GluRIA, Octα2R-Gal4*. Closed white arrow indicating four PENP neurons co-expressing *Octα2R* and *GluRIA*. Antibodies used: anti-GFP (green), anti-mCherry (red), and anti-SYN (blue). All scale bars = 50 μm unless otherwise specified

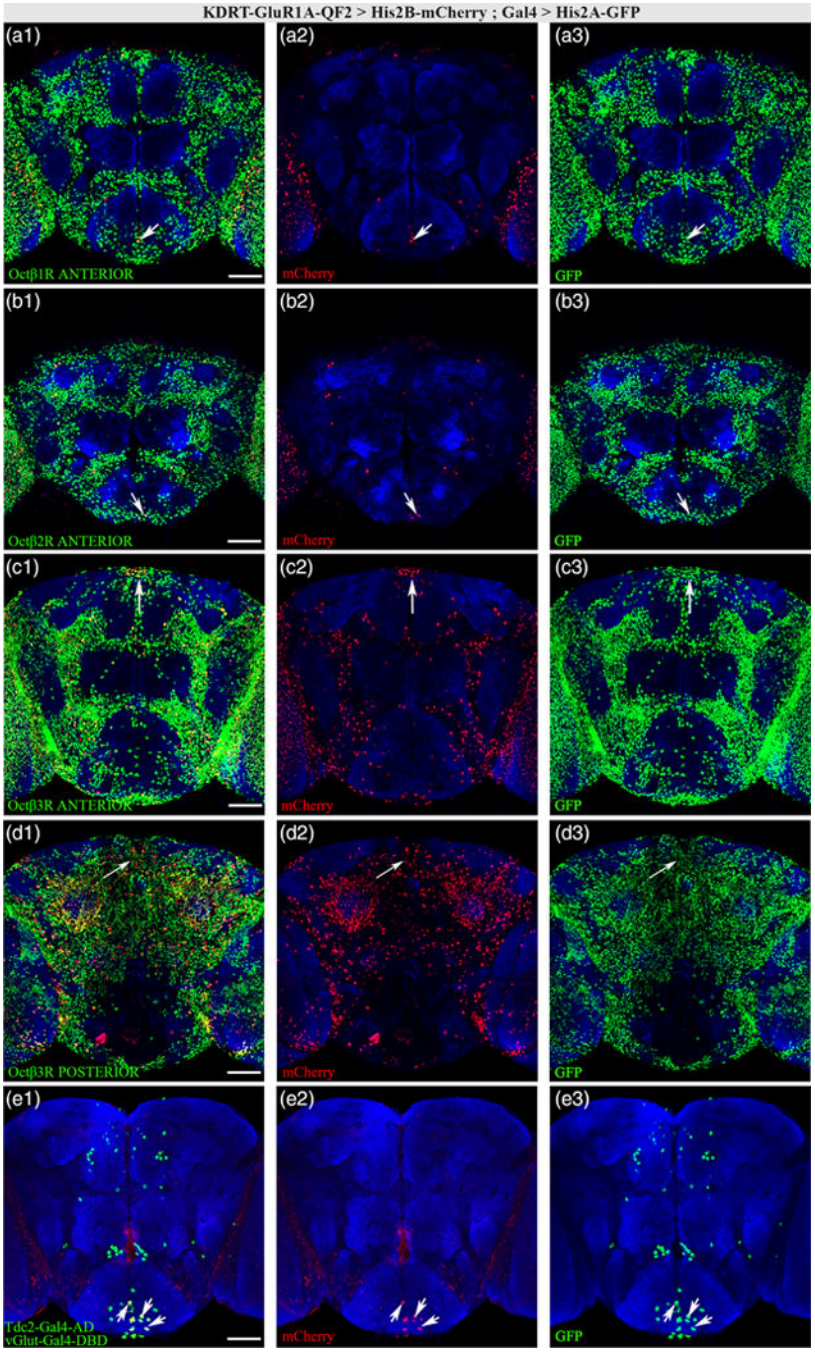

FIGURE 12.

KDRT-GluRIA expression in *OctβR-Gal4*s. (a1–a3) *yw; UAS-His2A-GFP, QUAS-His2B-mCherry; KDRT-GluRIA, UAS-KD/Octβ1R-Gal4* showing subset of *Octβ1R-Gal4* neurons in the anterior sections (a3, green) that also express *GluRIA* (a2, red), and merged channels (a1) with closed white arrow indicating at least one neuron co-expressing *Octβ1R and GluRIA in the anterior SEZ*. Very little co-expression was seen in the central brain, with the majority seen in the optic lobes. (b1–b3) *yw; UAS-His2A-GFP, QUAS-His2B-mCherry; KDRT-GluRIA, UAS-KD/Octβ2R-Gal4* labeling the subset of *Octβ2R-Gal4* neurons in the

anterior sections (b3, green) also expressing *GluRIA* (b2, red), and merged channels (b1) with closed white arrow indicating at least one neuron co-expressing *Octβ2R and GluRIA in the anterior SEZ*. (c1–d3) *yw; UAS-His2A-GFP, QUAS-His2B-mCherry; KDRT-GluRIA, UAS-KD/Octβ3R* anterior (c) and posterior (d) sections showing the subset of *Octβ3R-Gal4* neurons (c3, d3, green) also expressing *GluRIA* (c2, d2, red) and merged channels (c1,d1). Closed white arrows indicate co-expressing neurons in anterior and posterior superior medial protocerebrum. (e1–e3) *yw; UAS-His2A-GFP*, *QUAS-His2B-mCherry/Tdc2-Gal4-AD*, *vGlut-Gal4-DBD*; *KDRT-GluRIA, UAS-KD* labeling *GluRIA*-expressing neurons (e2) within the subset of neurons labeled by the *Tdc2*/*vGlut* split Gal4 (e3) and merged channels (e1). Closed white arrows indicate co-expressing neurons in the SEZ. Stained with anti-GFP (green), anti-mCherry (red), and anti-SYN (blue). Scale bars = 50 μm

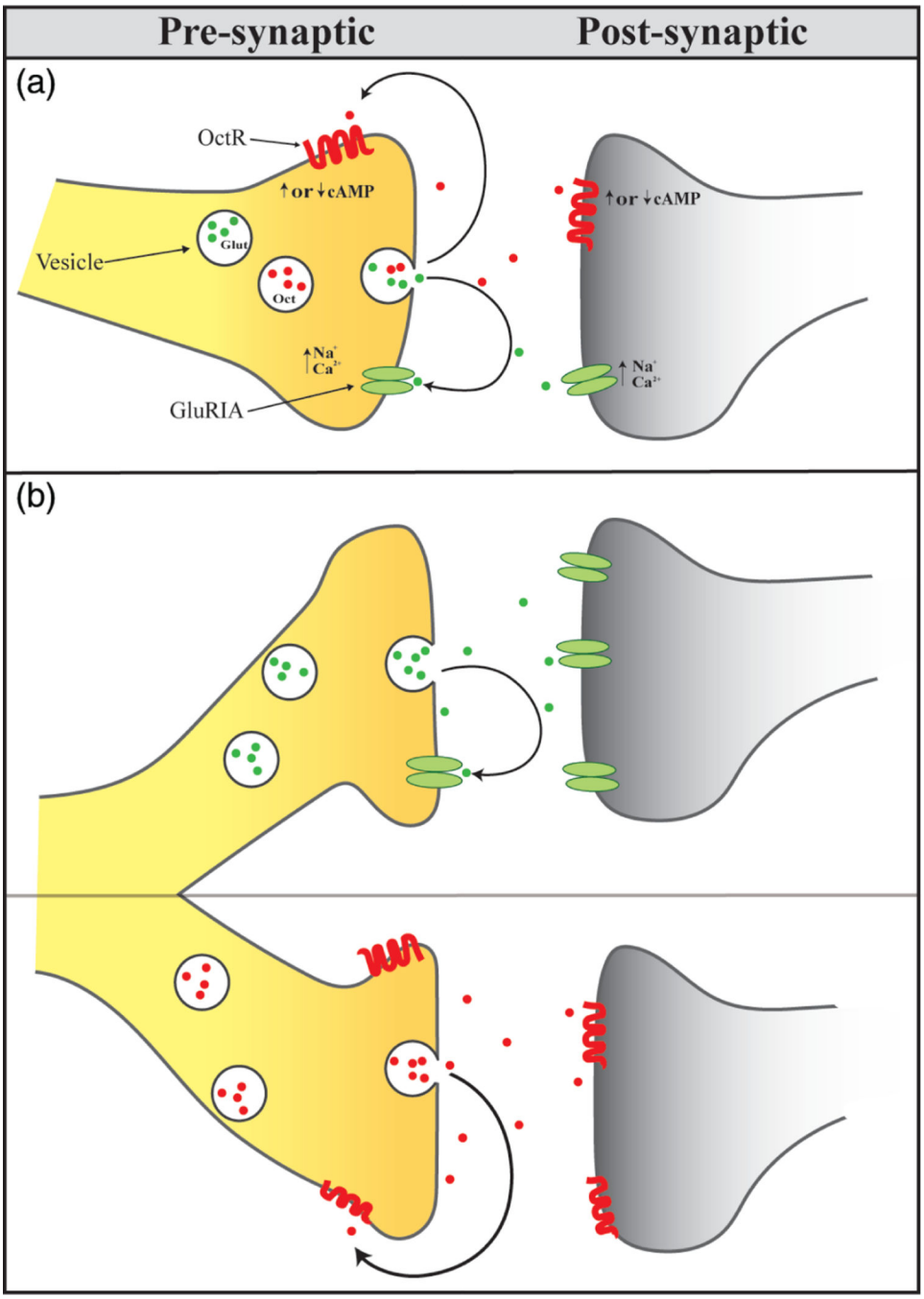

FIGURE 13.

Dual transmission and postsynaptic receptor scenarios. In dual transmitting neurons, neurotransmitters are either packaged in synaptic vesicles together (a, presynaptic) or separately (b,c, presynaptic) and may be released at the same synapse (a, presynaptic) or separate ones (b,c, postsynaptic). From our experiments here, we show OctR expression in Tdc2+ neurons, which are indicate autoreception properties as shown in (a) and (c). Additional data indicates potential GluRIA autoreception as seen in (a) and (b). Postsynaptically, receptors may be expressed together (a, postsynaptic) or on different

neurons (b,c, postsynaptic). Our data indicate a number of neurons express *OctR* and a *GluRIA*, as in (a)